



TECHNISCHE
UNIVERSITÄT
WIEN

DIPLOMARBEIT

Development of methods for corrosion inhibitor selection and quality assurance in oil and gas technology

Ausgeführt am Institut für
Institut für Chemische Technologien und Analytik
der Technischen Universität Wien

unter Anleitung von
Ao.Univ.Prof. Dipl.-Ing. Dr.techn. Paul Linhardt

durch
Seo Hee Son

Wien, Juli 2019

Contents

Abstract	iii
Acknowledgements	iv
1 Introduction	1
1.1 Motivation	1
1.2 Aim of the current work	3
2 Background and Literature Review	4
2.1 Corrosion	4
2.2 Faraday's law	7
2.3 Acid treatment	7
2.4 Corrosion inhibitors	8
2.4.1 Anodic corrosion inhibitors	9
2.4.2 Cathodic corrosion inhibitors	9
2.4.3 Mixed type corrosion inhibitors	10
2.5 Electrochemically measuring corrosion	10
2.5.1 Three electrode system	11
2.5.2 Electrochemical impedance spectroscopy (EIS)	11
2.5.3 Open circuit potential (OCP)	15
2.5.4 Potentiodynamic/galvanic polarization	16
3 Experimental	19
3.1 Weight loss experiments	19
3.1.1 At normal pressure in glass flasks	19
3.1.2 Autoclave experiments	21
3.2 Electrochemical methods	22
3.2.1 Sample preparation	22
3.2.2 Experimental set-up	24
3.2.3 Experimental procedure	27
3.3 Surface investigation	27
4 Results and Discussion	29
4.1 Weight loss measurements	29
4.1.1 Autoclave measurements	29
4.1.2 Blank measurements	31

4.1.3	Measurements with inhibitors	32
4.2	Polarization curves measurements	37
4.3	Open circuit potential (OCP)	41
4.4	Electrochemical impedance spectroscopy measurements	45
4.4.1	Repeatability- 0.1% inhibitor at room temperature without CO ₂	52
4.4.2	Repeatability- 0.1% inhibitor at 50°C without CO ₂	55
4.4.3	Repeatability- 0.1% inhibitor at room temperature with CO ₂	58
4.4.4	Repeatability- 0.5% inhibitor at room temperature without CO ₂	58
4.5	Surface	61
4.6	Experimental parameters	62
4.6.1	Adding inhibitors	63
4.6.2	OCP measurement	64
4.6.3	Cable setting	65
5	Conclusions	67
	References	69
	List of Figures	74
	List of Tables	78
	List of Abbreviations	79
	Appendix	80

Abstract

Corrosion of carbon steel in the oil and gas industry is a serious problem directly associated with economic loss and safety risks. As the equipment used in the industry is faced with corrosive environment, i.e. CO₂ or acidic conditions, corrosion inhibitors are applied in order to have corrosion under control. Since acid such as hydrochloric acid or acetic acid is widely used for the removal of scale in the equipment, there are corrosion inhibitors specifically against acids. Electrochemical methods have been widely used with the purposes of testing and analysing corrosion inhibitors.

The objective of this master thesis was to compare efficiency of various acid corrosion inhibitors under different experimental conditions using C1020 steel. The inhibition efficiency was studied by weight loss experiments and electrical impedance spectroscopy (EIS) at different temperatures and acid concentrations. Beside EIS measurements open circuit potential (OCP) measurements and potentiodynamic polarization measurements were carried out as well. OCP was the measure for the stability of the system and with polarization measurements statements about the modus of inhibitors could be made, whether they are anodic or cathodic or mixed type of inhibitors. Furthermore, scanning electron microscopy (SEM) was used to determine whether crevice corrosion has occurred, which would impact the EIS experiments and produce incorrect data.

Besides comparing the efficiency of inhibitors, an adequate method to improve the reproducibility of electrochemical impedance spectroscopy was developed. A few experimental parameters were varied in order to improve the repeatability, such as the duration of OCP measurement, stirring during the OCP measurement or the method of adding the inhibitor, either adding it directly, diluted in hydrochloric acid or in methanol.

Acknowledgements

I am grateful to OMV Exploration & Production GmbH in Gaenserndorf and Dipl.-Ing. Dr. techn. Gerald Zehethofer for the financial support.

I would like to express sincere gratitude to my supervisor Ao.Univ.Prof. Dipl.-Ing. Dr.techn. Paul Linhardt for his support and providing me with a precious opportunity to work on an interesting project for my master thesis.

Besides my supervisor, I also would like to thank Dipl.-Ing. Dr. techn. Sarah Hurch for supervising me at OMV Exploration & Production GmbH in Gaenserndorf with endless patience, support and immense knowledge. Furthermore, I would like to thank Dipl.-Ing. Dr. techn. Stefan Hoenig for the technical support and advice.

I am also grateful to Dipl. Ing. Guenther Ball who has helped me throughout my thesis.

Last but not least, I would like to thank my family for supporting me in every aspect of my life.

1 Introduction

1.1 Motivation

A study released in 2002 revealed that the U.S. spends \$276 billion to fight the consequences of corrosion which is approximately 3.1% of the nation's Gross Domestic Product (GDP) [1]. It is estimated that the corrosion costs \$4 trillion a year globally, which is comparable to damages caused by 40 Hurricane Katrina [2]. These costs cover prevention and control of corrosion as well as damages and lost productivity [2]. Moreover, in 1996 \$3.7 billion were spent in the petroleum industry in the U.S. for the same purpose [1]. Corrosion research is important not only from the economical view, but it is also in our interest because it is directly related to public safety as corrosion occurs from infrastructure (e.g. bridges, pipelines), to food processing, to transportation industry (e.g. motor vehicles, ships, aircraft) [1].

Corrosion is one of the biggest problems encountered in oil and gas industries, due to complexity of facilities, demanding production techniques and environmental and public safety threats in case components fail: In November 2013, a leaking oil pipeline caught fire in China and the explosion killed at least 62 people and wounded 136 [3]. Corrosion problems in oil and gas industry could occur at different stages in production, transportation and storage and/or various wells [4]. Since corrosion takes so many forms and is a natural process, it is almost impossible to prevent. However, there are various methods to control corrosion dependent on the used material and environment. It is crucial to understand corrosion mechanisms in order to monitor and prevent it.

Metal and metal alloys are the most widely used materials in various industrial applications, including the petroleum industry. Approximately 8% of the global production of metal is used for the petroleum industry [5]. The most common metal alloys are the ones with iron as the base element (ferrous alloys). Due to the low cost and material properties such as ductility, welding and forming abilities, carbon and alloyed steels are commonly used, except for cases where the operating condition is so severe, that higher grade materials must be used, such as nickel alloys or 28 Cr (Alloy 28) [6]. Carbon steel is used for pumps, valves, tubing and pipes; 98% of construction materials is made of carbon steel [4]. Despite its versatility, corrosion resistance of carbon steel is not always sufficient.

Corrosion is defined as the process of decay or deterioration of material caused by chemical or electrochemical reaction with the environment. There are conditions which need to be met so that electrochemical corrosion can occur:

- Metal
- Oxidant
- Electrolyte - electrically conducting solution, e.g. water.

Electrochemical corrosion is a redox reaction, in which reduction and oxidation take place simultaneously, when two different electric potentials come into contact with electrolyte - site where oxidants react will have more positive potential and site where metal oxidises to ions will have more negative potential.

It is well known that materials used in oil and gas industry are prone to corrosion due to severe conditions, e.g. high temperatures and pressures. The pressure can be increased to 15000 psi and beyond and the temperature to 350°C [6]. Furthermore, contaminants such as dissolved carbon dioxide (CO₂) and hydrogen sulfide (H₂S) cause sweet and sour corrosion respectively. Carbon steels are exposed to oxygen, salt, water and acids: Water injection - as one of the methods used to increase oil recovery from reservoir - and use of acids are one of the factors for this exposure. Corrosion caused by aforementioned factors is by far the most frequent form found in oil and gas production [7].

Although it is impossible to prevent metals from corrosion, there are methods to have it under control, through e.g. applying protective coatings, cathodic protection or using corrosion inhibitors. Among different methods for corrosion protection, corrosion inhibitors present an effective and flexible approach for corrosion control and is a standard method applied in oil and gas production [8][9]. Selection of inhibitors is complicated due to variability of corrosive environments, legal requirements and environmental concerns [8]. The type selection and the dosage of inhibitors depend not only on working conditions, such as acid used and its concentration, temperature and pH value but also on the material the inhibitors are supposed to protect. The first generation of acid inhibitors contained highly toxic organic arsenic compound [10] and was commonly used in mid-20th century [11]. However, due to formation of poisonous arsine gas under acidic conditions, organic arsenic compounds were replaced by inorganic salts and then subsequently by organic molecules containing N, O, P or S heteroatoms [12]. Most commonly used corrosion inhibitors are derivatives of carboxylic acid, amines, amides, imidazolines and sulfur - containing organic molecules [13]. How inhibitors protect metals is based mostly on interaction with a metal surface, forming a thin protection layer.

1.2 Aim of the current work

As corrosion inhibitors are crucial in oil and gas production from many aspects, the main aim of this work was to investigate the effectiveness of various acid corrosion inhibitors on carbon steel under a variety of conditions relevant to the oil industry. The experiments were carried out by means of weight loss and electrochemical experiments. Moreover, of particular interest of the project was to develop an electrical impedance spectroscopy method, which delivers reproducible results under the same circumstance. Developing such a method enables quality insurance of corrosion inhibitor, as the inspection of purchased inhibitors is facilitated.

2 Background and Literature Review

2.1 Corrosion

In wide sense corrosion is defined as degradation of a material, which includes metals and non-metallic materials such as polymers or ceramics. However, generally corrosion is taken as a natural process occurring between metal and its environment which leads to gradual destruction of metals by chemical or electrochemical reaction [14]. Corrosion for metals and alloys can be classified into three main categories [15]:

- Wet corrosion - As the name already refers, wet corrosion occurs when metals are exposed to an aqueous environment. The electrochemical processes takes place on the surface of the metals while the metals are converted into dissolved species or solid products [15].
- Corrosion in other fluids - Here corrosion arises in non-aqueous environment, such as molten salts or liquid metals [16][17]. This type of corrosion is not caused only due to electrochemical attack on metals, but also because of reaction between the metal alloy and the salt or the impurities in the salt [15].
- Dry corrosion - It is called also high temperature corrosion. When metals and alloys are exposed to aggressive gases or air, they undergo dry corrosion.

Generally the most common form among those three is the wet corrosion [15]. In an galvanic cell, chemical energy is converted into electrical energy. When metal is exposed to an aqueous environment, the liquid medium acts as an electrolyte. The electrode at which chemical oxidation occurs is known as anode. Generally the anodic reaction can be expressed as follows:



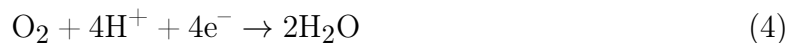
During the anodic reaction for iron, it loses electrons and becomes a positively charged ion:



The electrode at which chemical reduction occurs is known as cathode. The electrons released from the anode must be consumed simultaneously at the cathode and this can be done in various ways. Once electrons are produced from the anodic reaction, these can go through the the solid metal and reduce hydrogen ions to hydrogen gas (hydrogen evolution).



In an acidic solution with presence of oxygen, combination of hydrogen ions and electrons leads to reduction of hydrogen ions. As a result, the solution becomes less acidic:



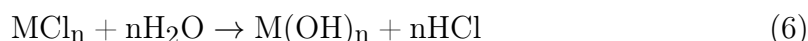
If the medium is neutral or basic, then it becomes more basic:



Despite the fact that cathodic and anodic reactions must happen simultaneously with the equivalent rate, it is usually recognized that the anode is where metal loss takes place [18].

Wet corrosion is most associated also in the oil and gas industry and the following lists a few types which are related to this work [19]: General corrosion, crevice corrosion, galvanic corrosion and sweet corrosion.

- General corrosion - It is also called uniform corrosion as the electrochemical reactions occur uniformly on the entire exposed metal surface. It can be relatively easily detected unless the corroding material is hidden from the sight. It is also considered less troublesome compared to other types of corrosion since the life of equipment can be estimated by determining its thickness (e.g. ultrasonic inspections).
- Crevice corrosion - Normally it is a localized attack, which arises in crevices or cracks between two joining surfaces [18]. The gap can be between metal and metal or metal and non-metal. Typically it can be found between a gasket and a metal surface [20]. Due to the geometry free access to the surroundings is limited, which leads to different concentration of chemical species such as oxygen and chloride: in the crevice there is low oxygen concentration because it is needed for the reaction (see equations 1 and 5) with metal and supply of more oxygen through the diffusion is restricted [18]. The crevice serves as anode and the surface above the crevice which has more access to the surroundings serves as cathode (see Figure 1). The chloride ions and metal ions form together metal chloride which can hydrolyse and eventually lowers the pH [21]:



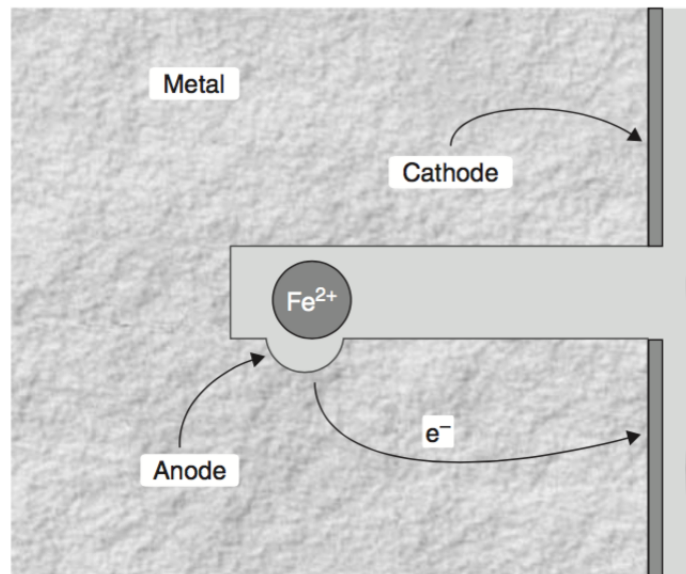


Figure 1: Schematic description of crevice corrosion [18].

- Galvanic corrosion - Also known as bimetallic corrosion, is induced when two materials of different electrochemical potentials are in electric contact in a corrosive electrolyte [18]. The less noble metal becomes an anode and corrodes and at the same time the more noble metal acts as the cathode and can be protected from corrosion. Figure 2 displays what galvanic corrosion looks like.

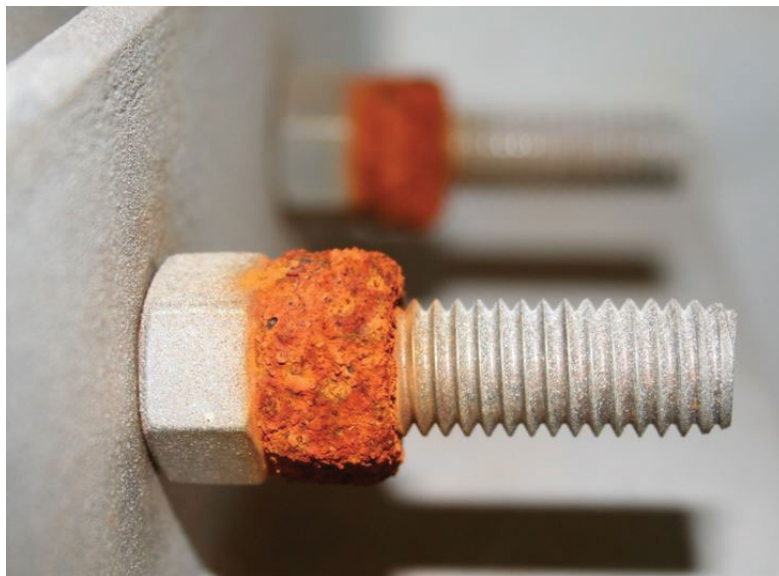


Figure 2: Galvanic corrosion [22].

- Sweet corrosion - CO_2 has been recognized as one of the main factors for corrosion in

the oil and gas production systems [23]. Carbon dioxide gas itself is not corrosive, however it becomes corrosive and promotes electrochemical reactions when it is dissolved in an aqueous medium forming carbonic acid [18]:



Carbonic acid can subsequently dissociate and hydrogen ions can be formed:



Since carbonic acid exists in solution only under the circumstance when it is in equilibrium with carbon dioxide, the concentration of the acid in the aqueous phase is lower than the concentration of CO_2 .

2.2 Faraday's law

If an anodic reaction takes place and an electric flow is promoted, this current can be converted into equivalent mass loss according to Faraday's law. Faraday's laws of electrolysis relate the amount of material produced and the number of electrons involved during an electrochemical reaction. Mathematically the law can be expressed as follows:

$$Q = F \cdot \Delta N \cdot n, \quad (10)$$

where Q is the charge, F is the Faraday number (96485 C/mol of electrons), ΔN the change in the number of moles and n the number of electrons per molecule of the species being reacted [18]. The total charge can be calculated by integrating the current over the time.

2.3 Acid treatment

Acid treatment, also called acidizing, is widely used in oil and gas industry to enhance the well productivity. It has been commercially available since 1932 and thanks to effective corrosion inhibitors the treatment is commonly used today [24]. The treatment utilizes injecting acids, such as hydrochloric acid, hydrofluoric acid or acetic acid in order to increase the permeability of the original reservoir through chemical reactions [25]. Acids react usually with calcite, limestone and dolomite in rocks and dissolve them, which leads

to enlarged flow channels.

Acids are also often used to remove scale and are applied when new wells are drilled and drilling mud has to be removed before the production starts [12]. These scale removal treatments are carried out with 15% HCl at approximately 60 °C [12]. As the acids are injected into the system through pipes made of steel, it is crucial to protect the pipes from the corrosive media.

2.4 Corrosion inhibitors

Corrosion inhibitors are added in low concentration (usually less than 1000 ppm [13]) to decrease the corrosion rate and reduce the metal dissolution. Commercially available corrosion inhibitors are a mix of different substances. It is generally agreed that the inhibitors in acid solutions are first adsorbed on the metallic surface and then act to retard the electrochemical corrosion process. As the inhibitors can react with the metal and environment in numerous ways, which can also occur simultaneously, it is difficult to assign one single mechanism to an inhibitor. The experimental conditions such as temperature, pH value, presence of other chemical species or nature of the acid have great influence on which mechanism would be dominant of all.

Inhibitors can be adsorbed on the metallic surface and the inhibitive efficiency is generally proportional to the surface coverage. However this cannot be applied to all inhibitors, because if some inhibitors are overdosed, such as thiourea and amines, they may enhance corrosion. There are a few factors which have impact on the surface coverage or adsorption of inhibitors:

- Physical adsorption - Due to the electrically charged metal surface or already adsorbed ionic species, inhibitor ions or molecules in solution can be adsorbed. Depending on the potential of the surface, different types of molecules are attracted: anions are drawn to a positively charged metallic surface.
- Chemisorption - Transition metals have vacant electron orbitals with low energy. This feature allows electron transfer between inhibitors and metal species and establish a coordinative type of link. Inhibitors with lone pair electrons or π -electron systems, e.g. aromatic rings are prone to form this type of "bond".
- Reaction of adsorbed inhibitors - Once the adsorbed species react with the metal, in some cases, they form products, which also have inhibitive effects (secondary inhibition). The efficiency of secondary inhibition may be lower or higher than the primary inhibition, therefore its effectiveness is decisive for the overall inhibitive

efficiency: for example, sulfoxides can be reduced to sulfides which have higher inhibitor efficiency.

- Interaction between adsorbed species.

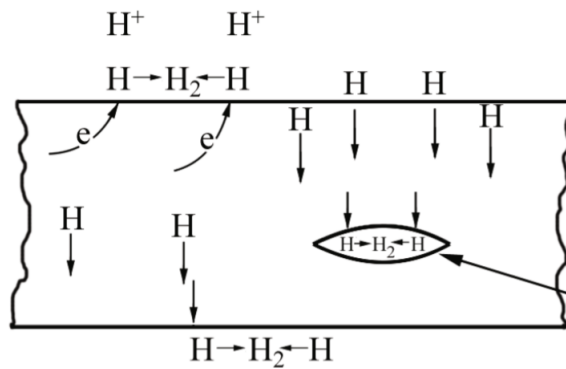
Corrosion inhibitors can be classified in many ways. They can be classified into (1) passivators, (2) organic inhibitors and (3) vapor-phase inhibitors or inorganic inhibitors, organic anionic and organic cationic.

2.4.1 Anodic corrosion inhibitors

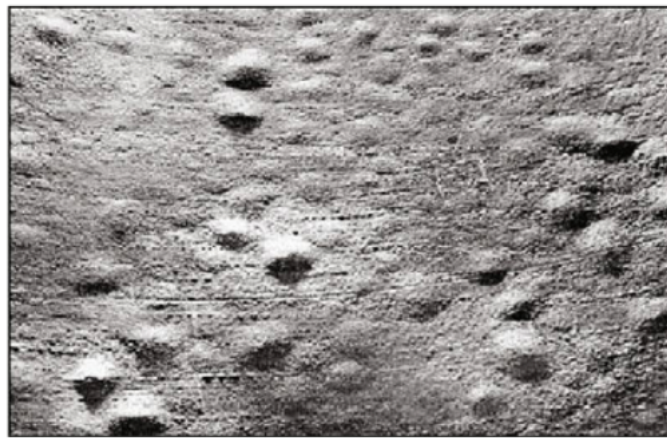
Anodic corrosion inhibitors (also known as passivating inhibitors) form a protective oxide film and stabilize the damaged passive film on the metal surface[26]. This protective insoluble film is formed, when anodic inhibitors react with the corrosion product [27]. As anodic corrosion inhibitors block the anodic reaction, the corrosion potential of the metal is shifted [27]. Chromates, nitrite and nitrate are oxidizing anions which are used as anodic corrosion inhibitors and they can passivate steel in the absence of oxygen [28]. Other types of anodic corrosion inhibitors are nonoxidizing ions and they passivate steel in the presence of oxygen - phosphate, tungstate and molybdatee can be classified to this type [29].

2.4.2 Cathodic corrosion inhibitors

Similar to anodic corrosion inhibitors, cathodic corrosion inhibitors act against corrosion by interfering with the cathodic reduction reaction (hydrogen gas evolution) and slowing the rate of cathodic reaction itself (cathodic poisons) [30]. Because both anodic and cathodic reactions have to occur at the same time, the whole corrosion process is retarded. However, the major drawback of this type of inhibition is the increase of susceptibility to hydrogen embrittlement. This is due to the increased concentration of hydrogen atoms on the surface since the recombination of hydrogen atoms is inhibited. The hydrogen atoms on the surface can be absorbed and diffuse into the metal and form blisters (see Figure 3)[30].



(a) Schematic illustration of formation of hydrogen blister [31].



(b) Hydrogen blisters on steel [31].

Figure 3

Another mode of action includes precipitation selectively on the cathode (cathodic precipitators), which leads to limiting the diffusion of oxidizing species [28].

2.4.3 Mixed type corrosion inhibitors

Besides cathodic and anodic corrosion inhibitors there are also mixed type corrosion inhibitors. Approximately 80% of organic compounds can be categorized as mixed inhibitors [29]. They affect both cathodic and anodic reactions. Typically they form a film so that anodic and cathodic surfaces are blocked (physical adsorption).

2.5 Electrochemically measuring corrosion

To determine corrosion rate weight loss measurements or electrochemically methods can be used. Weight loss measurements are cheaper and simpler to carry out, however it

requires longer experiment duration.

In this thesis three electrochemical techniques were used in order to compare the corrosion inhibitors and evaluate the electrolyte system: Open circuit potential (OCP), electrochemical impedance spectroscopy (EIS) and polarization method. Besides the EIS measurement, all measurements were done using a three electrode system, which is the most popular set-up in electrochemical studies [32].

2.5.1 Three electrode system

A three electrode system consists of working electrode, counter electrode and reference electrode (see Figure 4). The current travels between the working electrode and a counter electrode, also called auxiliary electrode. The potential of a reference electrode is known and as the name reveals already, the reference electrode acts as a reference in measuring the working electrode potential. The reference electrode should pass as little current as possible to ensure the reliable reference for potential control [32]. The reference electrode is positioned near to the working electrode in order to minimize solution resistance. Commonly used reference electrodes are Ag/AgCl electrode or saturated calomel electrodes.

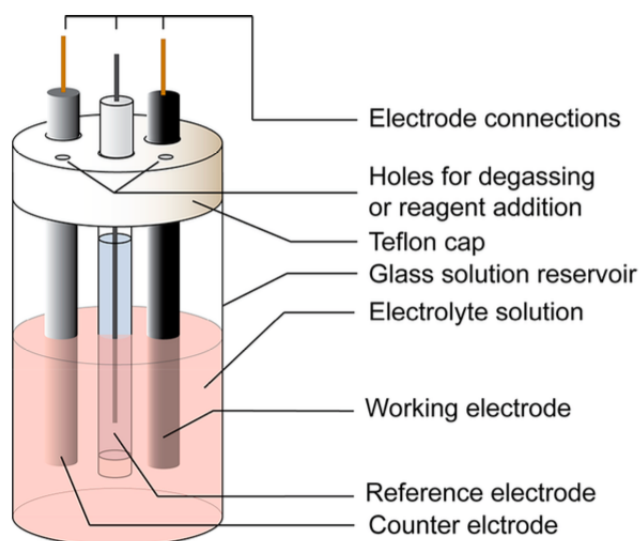


Figure 4: An illustration of a three electrode set-up [33].

2.5.2 Electrochemical impedance spectroscopy (EIS)

Electrochemical impedance spectroscopy has become a powerful electrochemical technique which is applied in a wide range of fields, including corrosion science, battery development and fuel cell testing [34][35][36]. Regarding oil and gas industry, EIS enables to investigate whether the corrosion inhibitor formed an adsorbed film or an organic

coating [37]. The principle of EIS will be explained following.

The Ohm's law is stated as:

$$R = \frac{V}{I} \quad (11)$$

where R is the electrical resistance [Ω], V the voltage or potential [V] and I the current [A]. The law describes the electrical resistance when the current goes through an electrical element. However, only one circuit element, the resistor can be described by this relationship, thus impedance Z should be used to describe more complex systems with capacitors or inductors [38]. Similar to resistance R , Impedance Z is the measure of resistance in a circuit when alternating current is applied.

Electrochemical impedance spectroscopy applies sinusoidal alternating voltage over a range of frequencies to an electrochemical cell, then the current through the cell is measured and analysed over the same range of frequencies, which is also an AC current signal [38]. However, the response can be shifted in phase or time, depending on the system measured (see Figure 5).

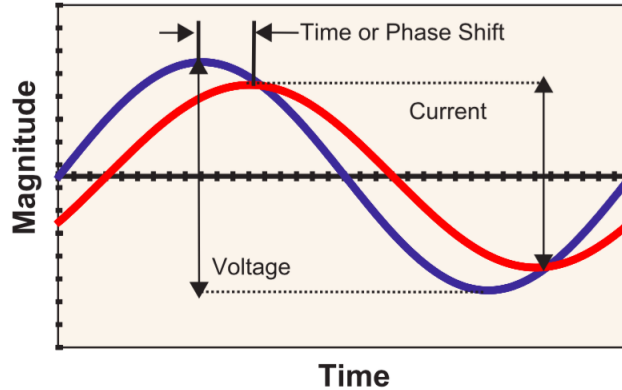


Figure 5: Delayed response [38].

The phase shift between the voltage and current waves can be expressed as an angle which is dependent on how much time one sine wave takes.

Mathematically impedance Z can be expressed as:

$$Z = \frac{V_{ac}}{I_{ac}} \quad (12)$$

V_{ac} is the excitation signal and I_{ac} is the current response. They can be described as follows:

$$V_{ac} = V_0 \exp(j\omega t) \quad (13)$$

$$I_{ac} = I_0 \exp(j\omega t - j\phi) \quad (14)$$

V_0 is the amplitude of the voltage, j the imaginary number, t the time, I_0 the amplitude of the current and φ the phase shift. ω is the angular frequency:

$$\omega = 2\pi f \quad (15)$$

Combining these equations and applying Euler's relationship (equation 16), the impedance can be separated into real and imaginary parts, shown in equation 17.

$$\exp(j\varphi) = \cos(\varphi) + j \sin(\varphi) \quad (16)$$

$$\begin{aligned} Z_{\text{real}} &= Z' = Z_0 \cos(\varphi) \\ Z_{\text{img}} &= Z'' = Z_0 \sin(\varphi) \end{aligned} \quad (17)$$

The φ is the phase angle, Z_{real} is the x-axis and $-Z_{\text{img}}$ is the y-axis of the Nyquist plot. The impedance is characterized by the magnitude of the impedance $|Z|$ (also called the modulus of the impedance), the phase and the frequency. To display EIS measurements Bode plots (see Figure 6) are often used, where these three parameters are plotted [38]. The frequency can vary from 100000 Hz to lower than 0.001 Hz, thus frequency (x-axis) is plotted logarithmically and the magnitude as well.

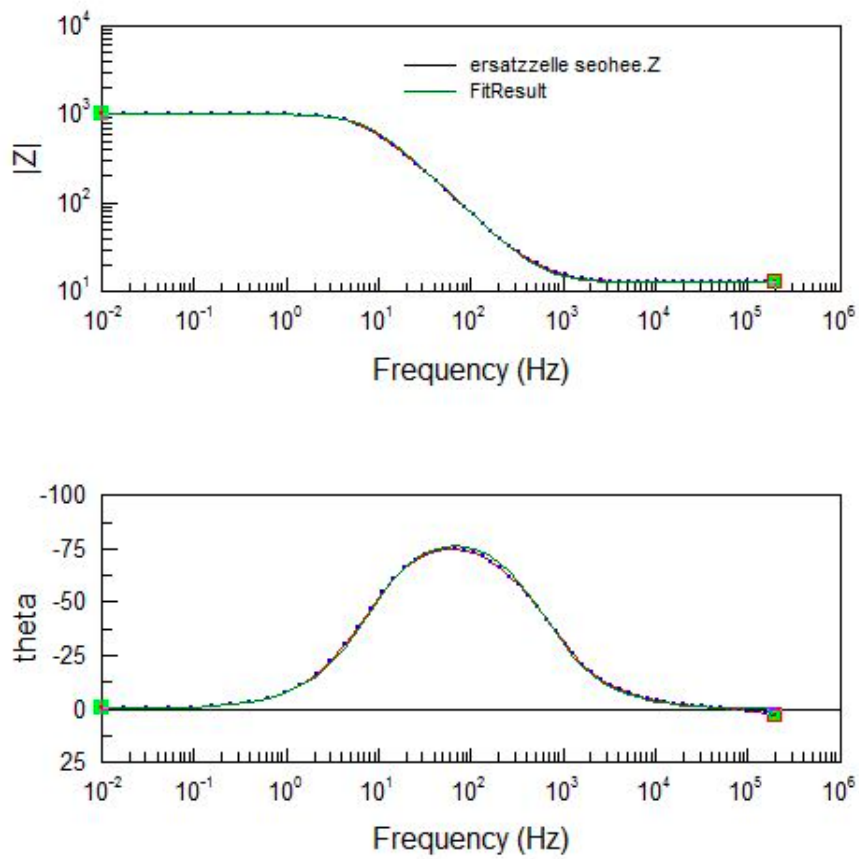


Figure 6: Typical Bode diagram. Frequency was varied from 0.01 Hz to 80160 Hz.

Another way of representing EIS data is by using a Nyquist plot. The x-axis and y-axis are real and imaginary part of the impedance respectively (see Figure 7).

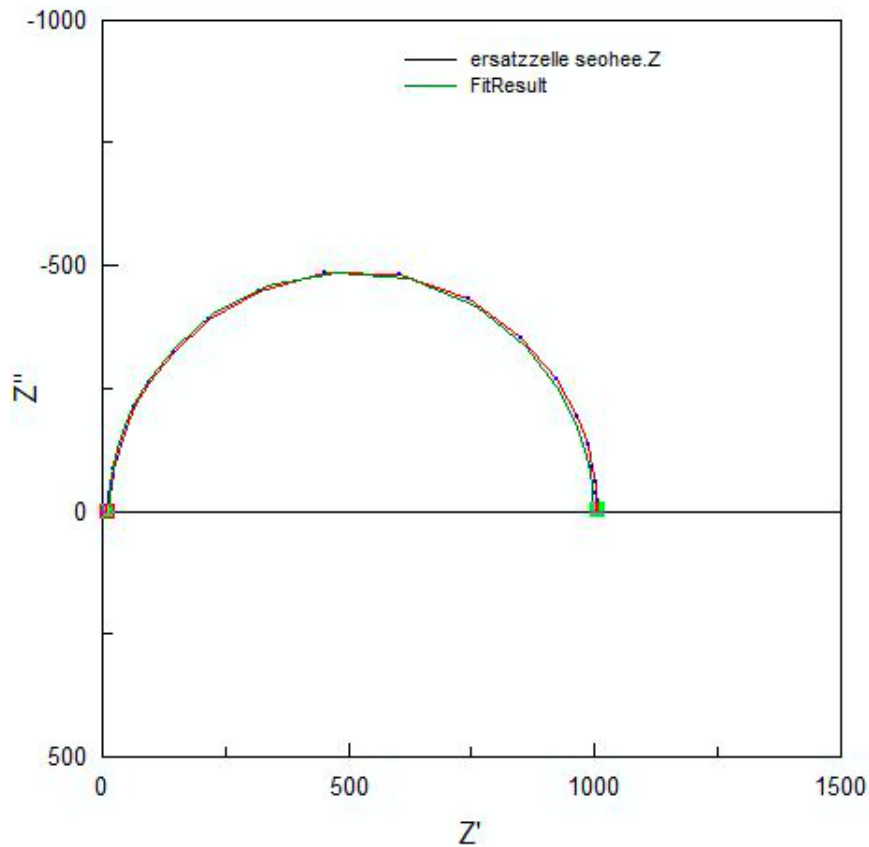


Figure 7: Nyquist plot. Frequency was varied from 0.01 Hz to 80160 Hz.

2.5.3 Open circuit potential (OCP)

An open circuit potential (OCP) refers to a circuit with no external current flowing through the cell [39]. It represents the potential difference between the working electrode and a reference electrode. It is also known as the equilibrium potential or corrosion potential E_{corr} . The value of corrosion potential depends and is a result of anodic and cathodic reactions [40]. E_{corr} can be shifted in positive direction when the current density of anodic reaction decreases or current density of cathodic reaction increases. Furthermore, it is crucial that the system has reached the quasi-steady state before beginning electrochemical experiments and OCP measurement allows to monitor the system in this respect. Figure 8 depicts the OCP vs. time during addition of a corrosion inhibitor in 15% hydrochloric acid at room temperature.

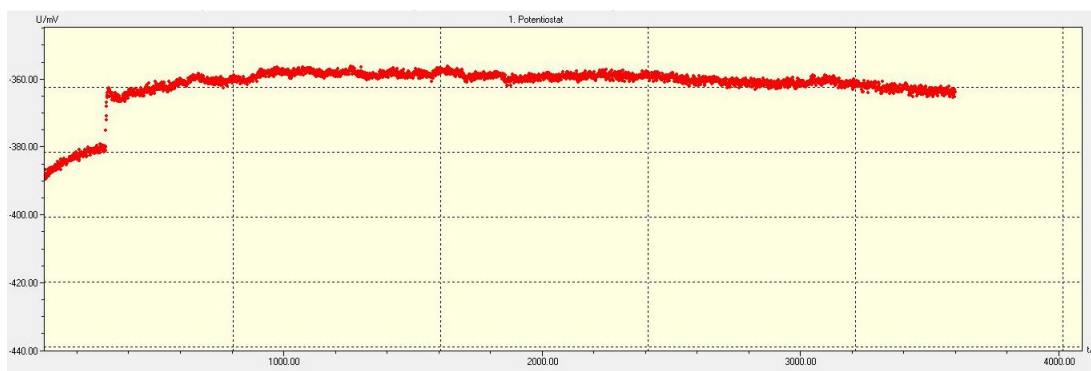


Figure 8: Open circuit potential as a function of time of an inhibitor in 15% HCl at room temperature.

2.5.4 Potentiodynamic/galvanic polarization

The electrodes are connected to the potentiostat. This device controls the potential of the working electrode (sample) and measures the current. Galvanostat, on the other hand, controls the current and measures the potential. During the potentiodynamic polarization the "equilibrium" corrosion process is perturbed due to the flow of current and the potential of working electrode is forced to shift from the E_{corr} . If the potential is forced to shift above the open circuit potential, then it is called "anodic polarization". In the other case, when the potential is shifted below the open circuit potential then it is called "cathodic polarization". When the logarithm of the absolute value of the current density, $\log |i|$ is plotted against the voltage E , then polarization curves can be plotted. Figure 9 shows polarization curves for iron in 1 M hydrochloric acid in absence of oxygen [41].

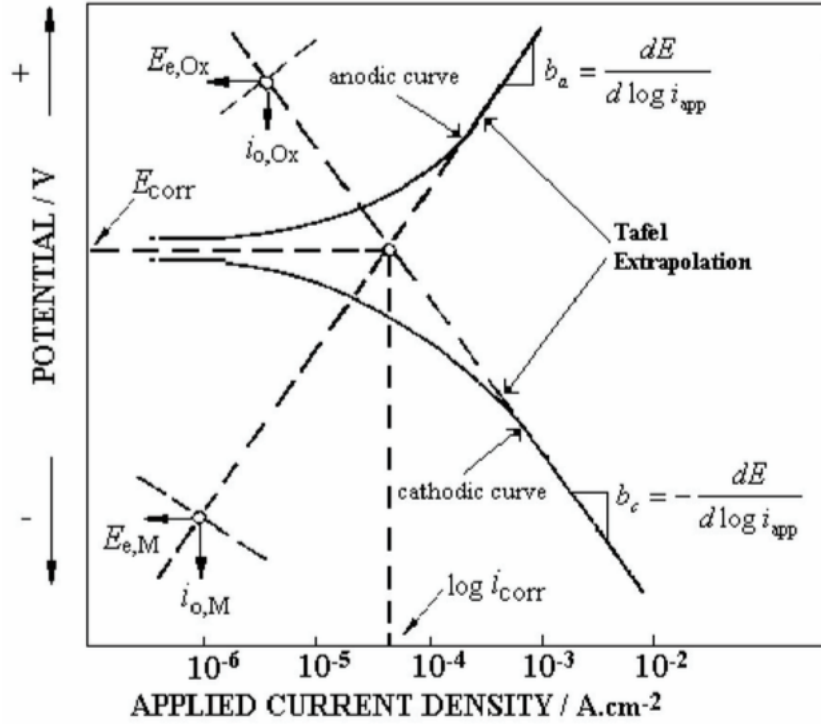


Figure 9: Polarization curves for iron in 1 M HCl in absence of oxygen [41].

With the polarization curves the corrosion rate can be determined by applying the Tafel extrapolation method. If the anodic and cathodic curves are linear (Tafel behavior) as shown in the Figure 9. They can be extrapolated back to zero overvoltage, which are called anodic and cathodic Tafel slopes. From the Tafel slopes Tafel constants b_a and b_c can be calculated. The intersection of these two slopes represents the corrosion potential E_{corr} and the corrosion current density i_{corr} . The Tafel extrapolation method is based on the Butler-Volmer equation:

$$i_{\text{net}} = i_{\text{corr}} \left[e^{\alpha n F (E - E_{\text{corr}}) / RT} - e^{-(1-\alpha) n F (E - E_{\text{corr}}) / RT} \right] \quad (18)$$

Tafel diagrams are useful to determine the efficiency of an inhibitor. It can be calculated by applying the following formula:

$$\text{IE}(\%) = \frac{I_{\text{corr}} - I_{\text{corr}}^*}{I_{\text{corr}}} \times 100, \quad (19)$$

whereas I_{corr} and I_{corr}^* are corrosion current density without and with the corrosion inhibitor respectively [42].

Tafel plots provide a fairly rapid method to determine corrosion current, which is related to corrosion rate. However, experimentally it is possible that the linear extrapolations

of anodic and cathodic polarization curves do not meet at E_{CORR} . One of the reasons for this is due to ambiguous linear Tafel regions, which leads to subjective interpretation of corrosion current value. Figure 10 shows potentiodynamic polarization curves, which are troublesome to lay definite extrapolation line on [43].

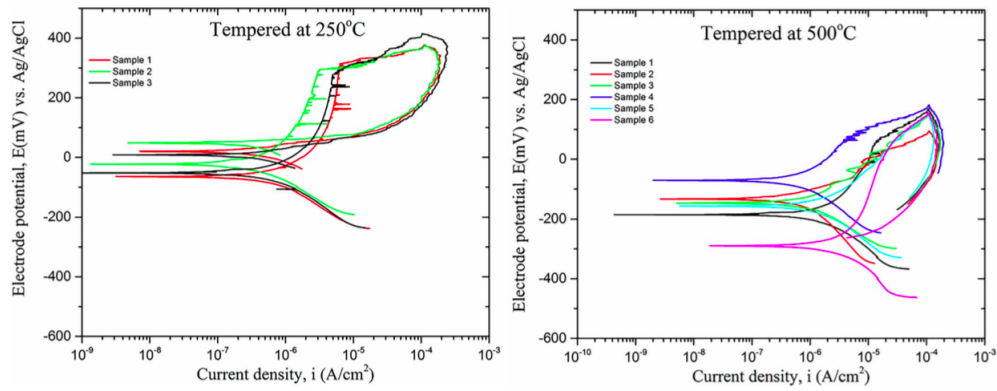


Figure 10: Potentiodynamic polarization curves of metals with different heat treatment [43].

3 Experimental

In this chapter details of procedure of executed experiments will be described including used equipments and chemicals. This includes softwares for the collection and analysis of potentiometric data. The metal coupon used for the study are a C1020 alloy.

3.1 Weight loss experiments

3.1.1 At normal pressure in glass flasks

- Without inhibitors: The metal samples were cut into the dimension of 60 x 16 x 1.6 mm³ and washed and brushed vigorously with a scouring agent before using. Afterwards, they were rinsed with tap water and acetone and dried with compressed air. The samples were weighed accurately before the measurement. Each coupon was immersed in a round bottom flask filled with a hydrochloric acid solution (250 ml), which had been submerged in a water bath (LAUDA ECO E 40 S, USA) at the desired temperature an hour before. After a certain amount of time the samples were taken out of the round flasks and were rinsed with tap water and acetone, dried with compressed air and weighed. These blank measurements were carried out with various concentrations of HCl solutions at different temperatures (see Table 1). Cooling fingers were placed on the flasks to avoid excessive evaporation of acid (see Figure 11).

	Temperature [°C]		
	25	55	77
HCl conc. [wt. %]	1 (3, 5.7)	1 (3, 5)	1 (3, 5)
(t ₁ , t ₂ [h])	8 (3, 5.7)	8 (3, 5)	8 (3, 5)
	15 (3, 5.7)	15 (3, 5)	15 (3, 5)
	28 (0.5, 1)	28 (0.5, 1)	28 (0.5, 1)

Table 1: Overview of executed blank measurements with varying temperature, concentration of medium and duration.

- With inhibitors: The dimension of used coupons was 126.6 x 16 x 1.6 mm³. For weight loss experiment with inhibitors 500 ml flasks were filled with 500 ml of 15 wt.% or 28 wt.% HCl solution. Concentrations of tested inhibitors were 0.1 vol.%, 0.5 vol.% and 2 vol.%. For the lowest concentration (0.1 vol.%), 5 ml of inhibitor was diluted in 45 ml hydrochloric acid solution, which has the same concentration as the testing medium. For the other two concentrations (0.5 vol.% and 2 vol.%)



Figure 11: Flasks with lids in the water bath.

inhibitors were added directly into the flasks with a pipette. After the addition, the flasks were shaken to achieve the maximum mixing of two different media. Then two coupons were immersed into one flask one after the other. Due to the gas formation during the corrosion process, the flask opening was sealed with Parafilm M and two holes were made with scissors (see Figure 12). The flasks were left in the fume hood and the temperature was kept at room temperature throughout the experiment. The overview of executed experiments can be shown in the Table 2.

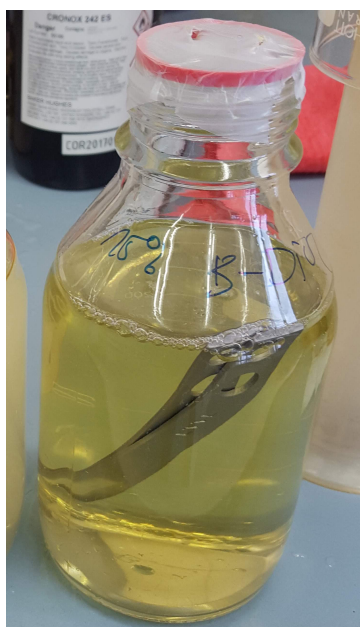


Figure 12: A flask containing two coupons submerged in 15 wt.% HCl solution and 0.1 vol.% butindiol and the sealed opening with two holes.

	HCl conc. [wt. %]	Inhibitor conc. [vol. %]	Time [h]
Exp. 1	15	0.1	64
Exp. 2	15	0.5	70.5
Exp. 3	28	0.1	79
Exp. 4	28	0.5	69
Exp. 5	28	2	70.5

Table 2: Overview of executed weight loss measurements with inhibitors.

Before and after the weight loss experiments with inhibitors, the metal samples were scrubbed with scouring agent, rinsed with acetone and dried with pressurized air before they were weighed.

3.1.2 Autoclave experiments

The autoclave experiments were planned and conducted by Michael Janka and Dr. Stefan Hoenig.

The metal coupons were prepared in the same manner as the weight loss experiments in glass flasks at normal pressure, placed on the sample holder made of PTFE and inserted to the autoclave (see Figure 13). Then the autoclaves were evacuated.



Figure 13: Components of an autoclave and the metal coupons on the sample holder.

Similar to the weight loss measurements the autoclaves are filled with the testing solution (pH=3 - Citrate buffer solution and osmose water) and 1000ppm inhibitor. Furthermore, gas (CO₂ at 20 bar or N₂ at 5 bar) was introduced at desired pressure in order to simulate the condition in which the metal coupons and the inhibitors are set in actual oil field. The autoclaves are set on the wheel in the drying chamber at 60°C (see Figure 14).



Figure 14: Autoclaves placed on the wheel apparatus.

The coupons were left in the autoclave for 5 days. After the experiment the metal coupons were scrubbed, rinsed with acetone and dried with pressurized air in the same manner as for the glass flask measurements.

3.2 Electrochemical methods

3.2.1 Sample preparation

Working electrodes and counter electrodes were prepared identically. Metal coupons of the dimension $126.6 \times 16 \times 1.6 \text{ mm}^3$ were prepared in the same manner as for weight loss experiments. However, further steps were necessary: coupons were polished with silicon carbide abrasive grinding paper of 320 grit (Struers, Austria) at 300 RPM with water on. The device used for polishing was RotoPol-31, Struers, Austria. Specimens were rinsed with acetone and dried with compressed air (see Figure 15).



Figure 15: Polished sample.

Polished coupons were then laid on a ruler and 1 cm above one end of a coupon was marked

with a pencil. Then approximately 0.5 cm above the mark a film (Scotchcal™ElectroCut™, 3M, USA) was attached to the coupon (see Figure 16)

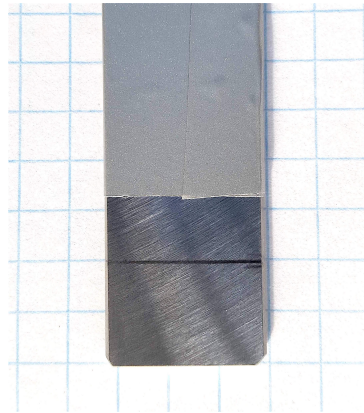


Figure 16: A coupon covered with a film.

The bottom 1 cm of a specimen was covered with polytetrafluoroethylene (PTFE) tape (see Figure 17a), in order to avoid contamination with the acrylic resin and to minimize contact with the air. Acrylic resin (VersoCit-2, Struers, Austria) was applied in the area between the PTFE tape and the film in order to avoid the direct contact of the film with the 15% HCl solution (see Figure 17b). VersoCit-2 powder and VersoCit-2 liquid were mixed in ratio of 1.5 to 1 by weight and the system was stirred until the mixture was homogeneous and it was applied on samples with a wooden stick. The applied resin was cured over the night in a fume hood.

The prepared coupon used for the EIS measurement is shown in the Figure 18.

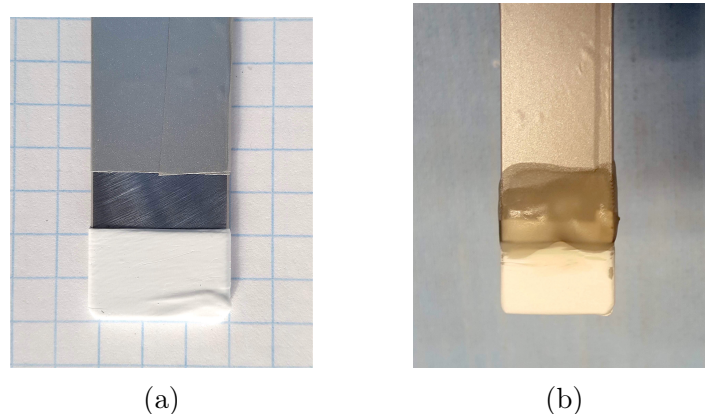


Figure 17: A coupon tip wrapped with PTFE tape and consequently applied resin.



Figure 18: A prepared coupon, which can be used for EIS measurements.

The working electrode and counter electrode had the surface area of 3.76 cm^2 .

3.2.2 Experimental set-up

All electrochemical measurements were performed within a glass double-wall jacketed cell, which had a plastic cover with openings for electrodes and gas in and outlets. The double-wall enables measurements at various temperatures, as it is connected to a thermostat (Fisher Scientific Polystat 36, USA). The test cell was located in a Faraday cage to shield the electromagnetic waves. The Faraday cage was connected to the potentiostat (IPS AJ), with which all the data of electrochemical measurements were obtained (see Figure 21). All electrochemical measurements were carried out either with purged CO_2 or open to the air.

As an electrolyte 500 ml of 15 wt.% HCl was used, for which 31 wt.% HCl solution (Donau Chem, Austria) was diluted with deionized water. Acid inhibitors were used as received. As a reference substance, 1,4-butindiol (99%, Sigma Aldrich, USA) solution was used (25 wt.% in ultrapure water). Polished carbon steels (prepared as described above in 3.2.1) were used as working and counter electrodes and they were mounted between half conical frustum shaped rubber parts and fixed with a metal string (see Figure 19). The electrodes were connected to the potentiostat using crocodile clamps. For linear polarization measurement platinum wire was used as a counter electrode (see Figure 20).



Figure 19: Electrodes mounted in conical frustum shaped rubber.



Figure 20: Platinum wire counter electrode for polarization curve measurements.

As a reference electrode a silver/silver chloride electrode (Sensortechnik Meisenberg GmbH, Germany) was used. The reference electrode was connected to a connector, which was filled with a 3 molar potassium chloride electrolyte solution (Metrohm AG, Switzerland). For each measurement the electrolyte solution from the previous measurement was removed from the connector and fresh solution was refilled without introducing any air bubbles. The whole set up can be seen in the Figure 21.

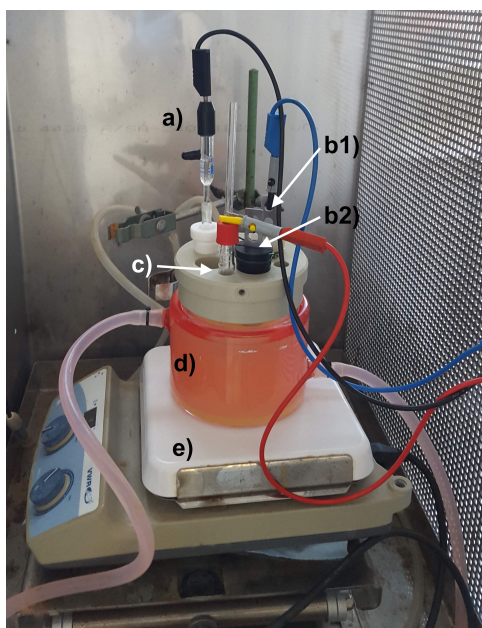


Figure 21: Experimental setup for polarization measurement : a) Ag/AgCl reference electrode, b1) counter electrode, b2) working electrode for EIS and OCP measurements, c) platinum wire counter electrode, d) glass double-wall jacketed cell, e) magnetic stirrer.

Measurements in CO_2 environment were executed after purging the electrolyte for one hour previously in order to obtain CO_2 saturated HCl solution. The gas was introduced and dispersed into the system through a gas washing bottle head with filter. For cleaning acetone and reverse osmosis water ran through the used gas washing bottle heads with filter through a pump (Watson Marlow 323 Peristaltic Pump, USA, see Figure 22).



Figure 22: Cleaning gas washing bottle head with acetone using a pump.

3.2.3 Experimental procedure

The working electrode and the counter electrode were immersed 1 cm into the electrolyte for 20 min to establish quasi steady state before starting measurements, while the system was stirred with a magnetic stirrer. Blank electrochemical impedance spectroscopy measurements were carried out within frequencies from 80160.3 Hz to 0.01 Hz, whereas an amplitude of 10 mV AC signals was used.

After the blank EIS measurement open circuit potential (OCP) measurement took place for an hour, during which the system was stirred with a magnetic stirrer. Acid inhibitor was added 5 minutes after the beginning of OCP measurement, either directly with a pipette or diluted in methanol or HCl. When a pipette was used for the dispensing inhibitor into the electrolyte, the tip did not touch the surface of the electrolyte solution. Moreover, due to the viscosity of acid inhibitors, only the necessary depth of a tip was immersed during aspirating the liquid. During OCP measurements changes in potential over the time was recorded. Once OCP measurement was terminated, the magnet stirrer was turned off and unplugged and the EIS was carried out three times consecutively within the same frequency range as the blank measurement. The potentiodynamic polarization measurements were performed in the potential range of -600 mV to -100 mV. Cathodic and anodic branches were measured with two separate coupon pairs. The potential was plotted versus logarithm of corrosion current density I (versus Ag/AgCl reference electrode) with a scan rate of 0.1 mV/s.

The acquired electrochemical impedance data were analyzed using the impedance fitting software Zview.

3.3 Surface investigation

Samples after the OCP, EIS and polarization measurements were put under a microscope to have a closer look on the surface underneath the acrylic resin, in order to check whether crevice corrosion has occurred during the electrochemical measurements. The samples were cut slightly above the film and put on a sample holder (see Figure 23).



Figure 23: Cut sample and the sample holder.

The sample and sample holder were placed on the sample chamber with resin for mounting (CitoPress-5, Struers, Austria). The mounting parameters were as following: 150°C, 300 bar and 5 minutes. Once the mounting process was finished (see Figure 24a), the sample was grinded to remove the upper 1mm layer (MD-Piano 80, Struers, Austria) and consequently polished with a series of resin bonded diamond discs with decreasing particle size (MD-Piano 120, and MD-Allegro Struers, Austria) and DP-Spray P 9 and 6 μm (Struers, Austria) were spread on the discs before the polishing. Finally, the polished sample (see Figure 24b) was put under the microscope and pictures were taken.



(a)



(b)

Figure 24: Mounted sample before and after the polishing.

4 Results and Discussion

4.1 Weight loss measurements

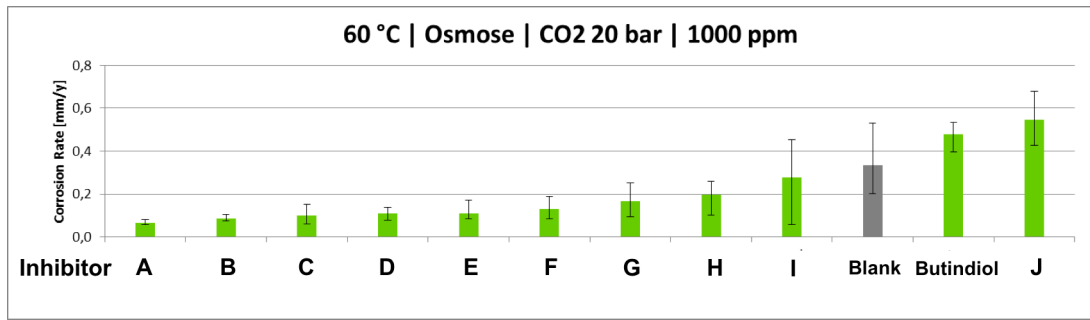
4.1.1 Autoclave measurements

The autoclave experiments were executed in order to study the effect of lower pH on inhibitor efficiency. One experiment was carried out in pH3-Buffer with nitrogen pressure of 5 bar and the other experiment in osmose water with 20 bar of carbon dioxide. In both cases inhibitors were added with 1000 ppm. The results of the autoclave experiments are represented in the Figure 25.

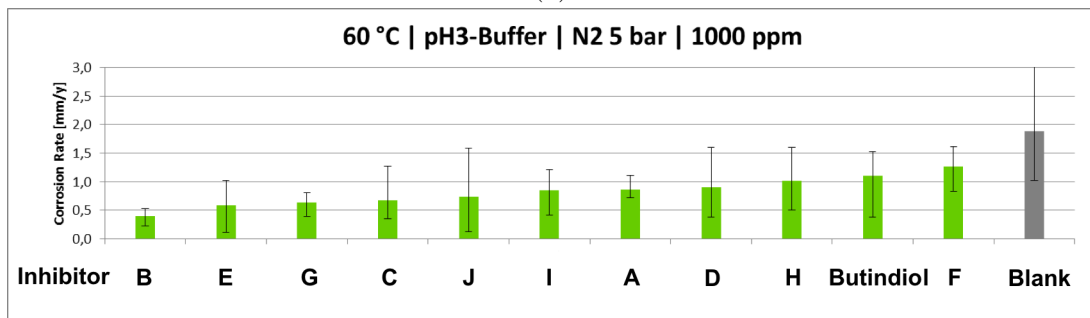
In osmose water with CO₂ and a theoretical pH value of 3.27, Inhibitor A had the lowest corrosion rate lower than 0.1 mm/y. Inhibitor B ranked as the second best, however the best seven (Inhibitor A, B, C, D, E, F, G) out of tested ten inhibitors showed comparable result with corrosion rate lower than 0.2 mm/y. Inhibitor I was only slightly better than blank. One inhibitor (Inhibitor J) showed higher corrosion rate than blank values, in other words, this inhibitor even promotes corrosion of metal coupons. This inhibitor was disqualified from further tests.

In pH3-Buffer Inhibitor B had the lowest corrosion rate with lower than 0.5 mm/y. From the seven inhibitors with the lowest corrosion inhibitors (Inhibitor A, B, C, E, G, I, J) in this experiment, five of them (Inhibitor A, B, C, E, G) were already included in the best seven from the osmosis experiment. Unlike experiments done in osmosis water, in pH3-Buffer solution all inhibitors were proved to have lower corrosion rate than the blank value. Furthermore, Inhibitor I had the lower range of corrosion rate in pH3-Buffer experiment unlike in osmosis water with 20 bar of CO₂. Besides the corrosion rate, parameters such as toxicity of inhibitors were taken into account. The choice of inhibitors for further studies includes butindiol, as a simple reference substance. It is known for its corrosion inhibition characteristics [44]. Moreover, the rank of inhibitors according to corrosion rate varies as the experimental condition changes. Therefore, a few inhibitors with the lowest corrosion rate from both experiments were taken into account, which are Inhibitor B, C, D, E and I.

Despite the comparable pH value of the two experimental condition, the overall corrosion rate in the experiment in osmosis water is lower than the other. This can be attributed to the presence of chloride ions (in the pH3-Buffer solution), which are thought to be necessary for the corrosion initiation as they can de-passivate passive films due to their small radius [45]. Furthermore, several publications suggest that chloride ions have remarkable influence on the protective efficiency of ferrous metal [46].



(a)



(b)

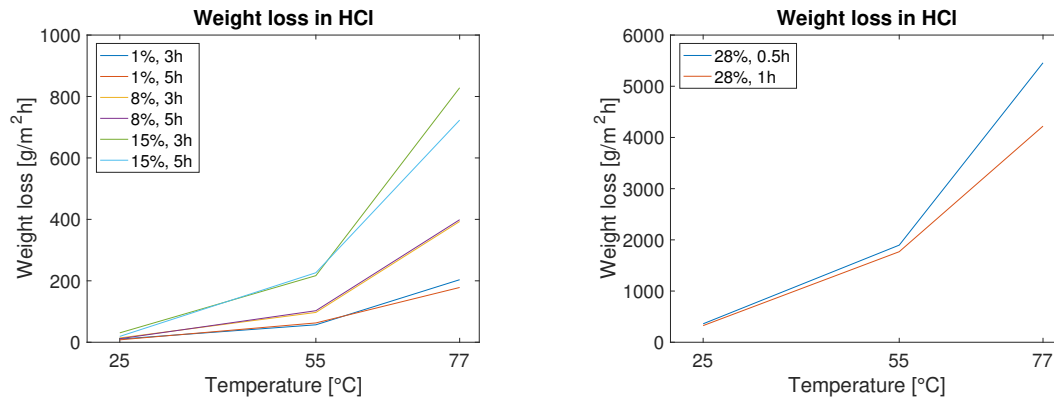
Figure 25: Autoclave experiments in two different medium: (a) osmosis water with 20 bar CO₂ (no Cl⁻ present), (b) pH3-Buffer with 5 bar N₂ (Cl⁻ present).

4.1.2 Blank measurements

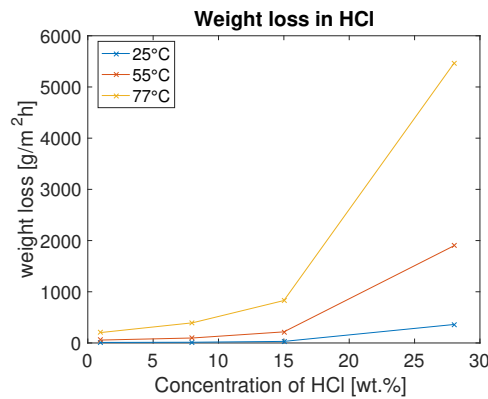
The weight loss of metal specimens after the exposure to 1%, 8%, 15% and 28% HCl for a certain amount of time was calculated in g/m²h. The result is illustrated in Figure 26, which shows clearly that the elevation of temperature and higher concentration of the media enhance the weight loss. As expected no linear relationship between temperature and weight loss was observed. It is well known that the corrosion rate can generally be described by the Arrhenius equation, which suggests the corrosion rate follows the shape of exponential function and inverse of absolute temperature [47]:

$$k = A * \exp^{-\frac{E}{RT}} \quad (20)$$

where k stands for the rate, A the proportionality constant, E the activation energy (J/mol), R the gas constant (8.314 J/mol K) and T the absolute temperature (K). Moreover, it can be seen (Figure 26c) that the higher the temperature is, the change of concentration has more severe impact on metal coupons. It was observed that increased exposure time leads to decreased corrosion rate, which can be noticed especially well at higher temperature. This decrease in corrosion rate can be explained by reaching the chemical equilibrium, as more and more Fe ions are dissolved in the solution. Furthermore, as corrosion proceeds hydrogen atoms evolve on the surface of the metal and they would disturb oxidants to reach the metal.



(a) Weight loss [g/m²h] at various temperature and HCl concentrations. (b) Weight loss [g/m²h] at various temperature at 28% HCl concentrations.



(c) Variation of weight loss [g/m²h] at different temperatures as a function of concentration.

Figure 26

4.1.3 Measurements with inhibitors

For the comparison of inhibitors inhibitor efficiency (IE) was calculated using the following formulas:

$$\nu = \left(\frac{W_1 - W_2}{ST} \right) \quad (21)$$

$$IE(\%) = \left(\frac{\nu_0 - \nu}{\nu_0} \right) \cdot 100 \quad (22)$$

where ν is the corrosion rate, W_1 and W_2 are the weight of coupons before and after the experiment respectively. S is the surface area and T is the immersion time. ν_0 was obtained from the blank measurements and ν from the measurements in the presence of inhibitors. The results are depicted in the Figures 27 to 30. It is noticeable, that the increase of inhibitor concentration changes the IE the most in case of butindiol, regardless

of HCl concentration and the temperature. Inhibitor E on the other hand shows the least change of IE, when it is added in lower or higher concentration into 15 and 28% HCl solution. This indicates butindiol is underdosed.

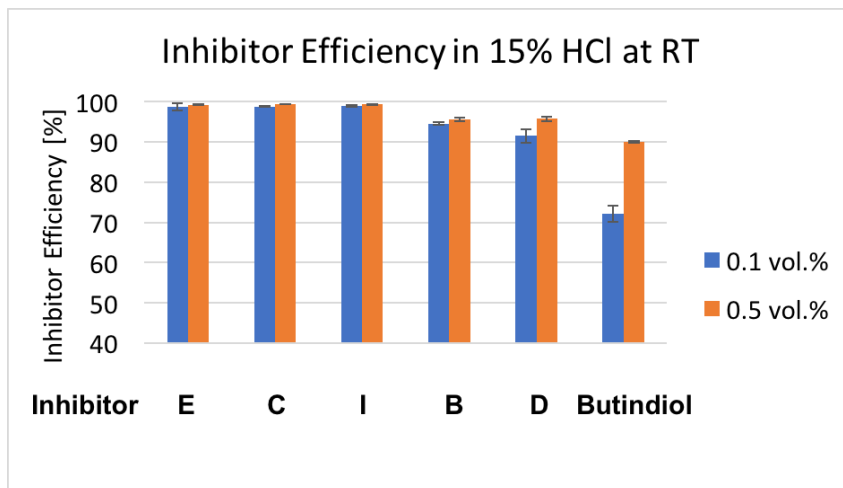


Figure 27: Inhibitor efficiency in 15% HCl in room temperature. The tested concentrations of inhibitors were 0.1 vol.% and 0.5 vol.%.

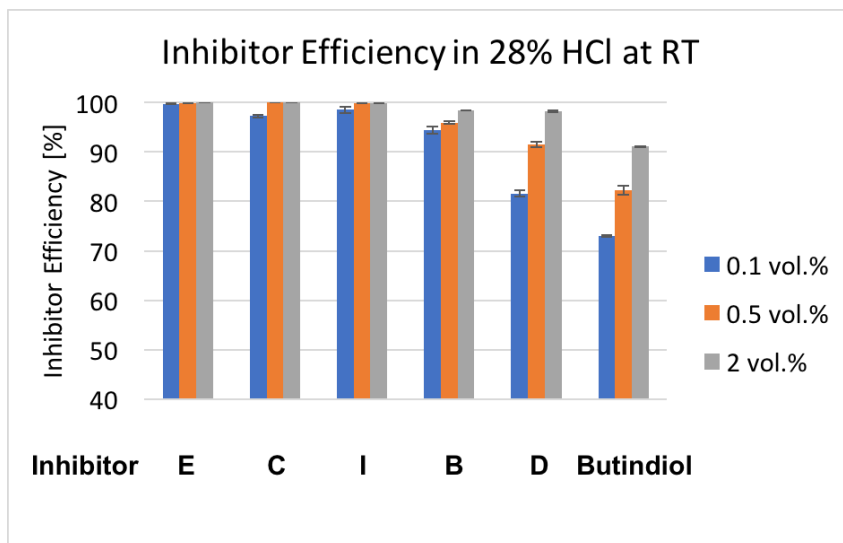


Figure 28: Inhibitor efficiency in 28% HCl in room temperature. The tested concentrations of inhibitors were 0.1 vol.%, 0.5 vol.% and 2 vol.%.

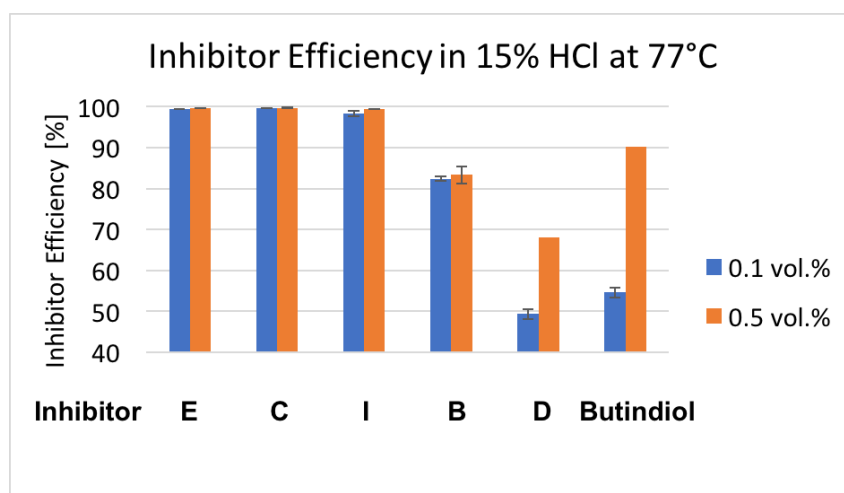


Figure 29: Inhibitor efficiency in 15% HCl at 77°C. The tested concentrations of inhibitors were 0.1 vol.% and 0.5 vol.%.

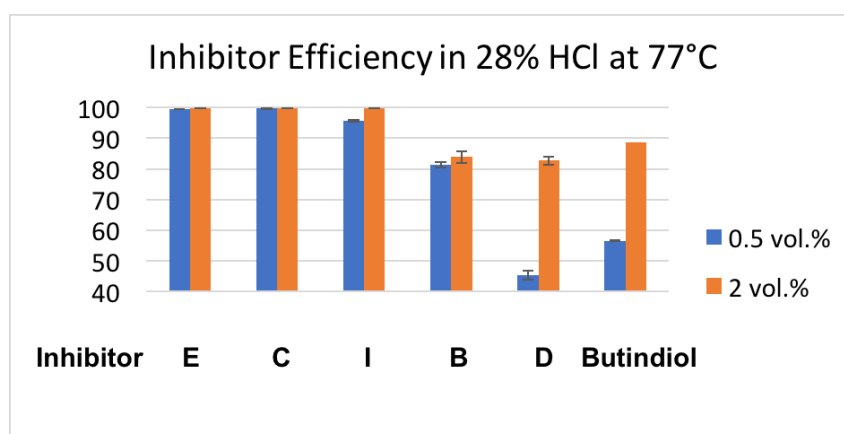


Figure 30: Inhibitor efficiency in 28% HCl at 77°C. The tested concentrations of inhibitors were 0.5 vol.% and 2 vol.%.

It is worth noting, that the performance of Inhibitor D decreases dramatically, when the temperature is elevated to 77°C, its performance is even lower than the reference substance butindiol. However, it should be taken into account, that butindiol was diluted 25 wt.% and once again diluted to either 0.1 vol.%, 0.5 vol.% or 2 vol.%, whereas the inhibitors were diluted directly from the mother solution. Furthermore, it should be mentioned that Inhibitor B also shows corrosion inhibition properties in every executed experiment even better than some "acid corrosion inhibitors". This inhibitor is sold as a "normal" oil field inhibitor and is usually used to prevent CO₂ corrosion. Inhibitor C, E and I are the three best inhibitors in all executed experiments. Results of experiments at room temperature show inhibitor efficiency of these three inhibitors are over 98%,

apart from Inhibitor C with 97.28% (0.1 vol.% in 28 % HCl). Inhibitor E has only slight improvement in IE when the concentration is increased from 0.1 vol.% in 15 % HCl and 28 % HCl. Even though the inhibitor efficiency is more or less the same within the three inhibitors, by looking at their corrosion rates Inhibitor C is the best corrosion inhibitor at room temperature. When it was dosed with 0.5 vol.% (in 15 %HCl and 28% HCl) it had the least corrosion rate and the corrosion rate was more or less the same when it was dosed at 0.5 % or 2 %.

Experiments carried out at 77°C proved Inhibitor C was the best inhibitor with the lowest corrosion rate and the highest IE. The second best was Inhibitor E. However, its corrosion rate is the double of Inhibitor C. Inhibitor D has even lower IE than the reference substance butindiol and proves to be not adequate as acid corrosion inhibitor at higher temperature.

The corrosion rate and inhibitor efficiency of each inhibitor are shown in the Tables 3 - 6.

Inhibitor	0.1 vol.%		0.5 vol.%	
	ν [g/m ² h]	IE [%]	ν [g/m ² h]	IE [%]
Inhibitor B	1.37	94.49	1.09	95.60
Inhibitor C	0.29	98.83	0.15	99.38
Inhibitor D	2.11	91.52	1.07	95.71
Inhibitor E	0.34	98.63	0.18	99.26
Inhibitor I	0.25	98.98	0.16	99.37
Butindiol	6.90	72.22	2.49	89.90

Table 3: Corrosion rate ν and inhibitor efficiency of C1020 alloy in 15% HCl at room temperature. The tested concentrations of inhibitors were 0.1 vol.% and 0.5 vol.%.

Inhibitor	0.1 vol.%		0.5 vol.%		2 vol.%	
	ν [g/m ² h]	IE [%]	ν [g/m ² h]	IE [%]	ν [g/m ² h]	IE [%]
Inhibitor B	19.30	94.37	15.05	95.90	5.33	98.45
Inhibitor C	9.29	97.29	0.09	99.97	0.08	99.98
Inhibitor D	63.26	81.55	29.21	91.48	5.89	98.28
Inhibitor E	1.01	99.70	0.22	99.93	0.10	99.97
Inhibitor I	4.91	98.57	0.47	99.86	0.21	99.94
Butindiol	92.94	72.95	60.76	82.28	30.56	91.09

Table 4: Corrosion rate ν and inhibitor efficiency of C1020 alloy in 28% HCl at room temperature. The tested concentrations of inhibitors were 0.1 vol.%, 0.5 vol.% and 2 vol.%.

Inhibitor	0.1 vol.%		0.5 vol.%	
	ν [g/m ² h]	IE [%]	ν [g/m ² h]	IE [%]
Inhibitor B	174.14	82.37	164.87	83.31
Inhibitor C	2.99	99.70	2.80	99.72
Inhibitor D	499.74	49.40	314.50	68.15
Inhibitor E	6.34	99.36	4.13	99.58
Inhibitor I	16.24	98.36	5.36	99.46
Butindiol	118.51	54.58	96.74	90.20

Table 5: Corrosion rate ν and inhibitor efficiency of C1020 alloy in 15% HCl at 77°C. The tested concentrations of inhibitors were 0.1 vol.% and 0.5 vol.%.

Inhibitor	0.5 vol.%		2 vol.%	
	ν [g/m ² h]	IE [%]	ν [g/m ² h]	IE [%]
Inhibitor B	850.03	81.25	731.51	83.87
Inhibitor C	14.67	99.68	3.64	99.92
Inhibitor D	2482.2	45.26	781.74	82.76
Inhibitor E	28.39	99.37	8.72	99.81
Inhibitor I	199.95	95.59	7.51	99.83
Butindiol	1966.9	56.62	513.25	88.68

Table 6: Corrosion rate ν and inhibitor efficiency of C1020 alloy in 28% HCl at 77°C. The tested concentrations of inhibitors were 0.5 vol.% and 2 vol.%.

4.2 Polarization curves measurements

Polarization curve experiments were conducted as the last step of an experiment with one set of metal coupons, as it is a destructive method, since corrosion is forced on the working or counter electrode depending on the anodic or cathodic measurement. Current response is recorded against the potential and it allows the study of anodic (dissolution of mild steel) and cathodic (hydrogen evolution) responses. The experiment was conducted as described in the chapter 3.2.3.

Tafel polarization curves for C1020 alloy steel in 15% HCl solution with two inhibitor concentrations (0.1 vol.% and 0.5 vol.%) at room temperature are shown in Figure 31 and 32. It can be seen clearly in both figures, that the addition of inhibitors decreases the values of anodic and cathodic current density, which suggests that the tested inhibitors are mixed-type inhibitors. It is noticeable in both figures, that the anodic curve of Inhibitor I has significantly lower values of current density than the other inhibitors, suggesting that this inhibitor prevents anodic reaction more effectively compared to the others. Similarly, increase of concentration leads to higher protection of steel with both cathodic and anodic reaction suppression (see Figure 33) It is worth noticing in Figure 33c, that higher concentration of Inhibitor I leads to significant shift of E_{CORR} to higher potentials, resulting in higher resistance to corrosion.

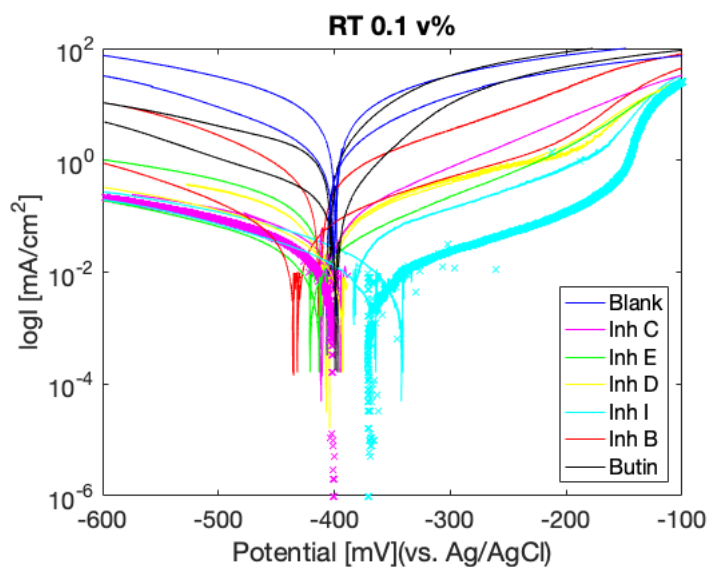


Figure 31: Tafel polarization curves of different inhibitors with 0.1 vol.% measured at room temperature in the open air without CO₂.

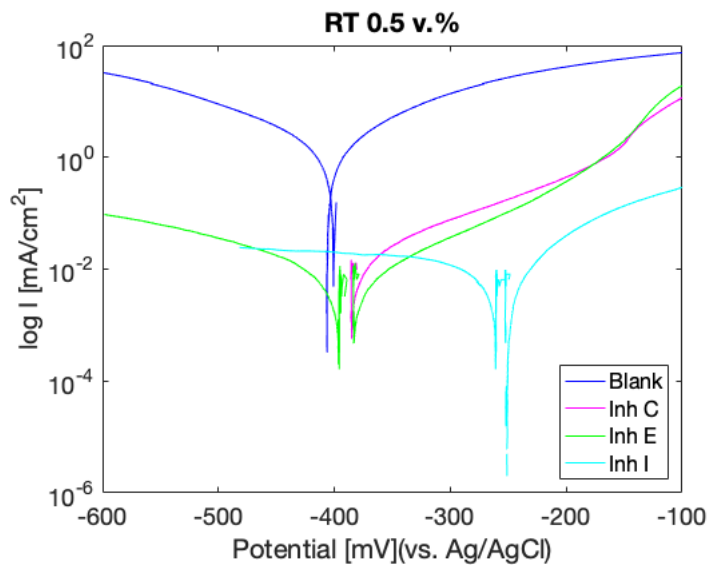


Figure 32: Tafel polarization curves of different inhibitors with 0.5 vol.% measured at room temperature in the open air without CO₂.

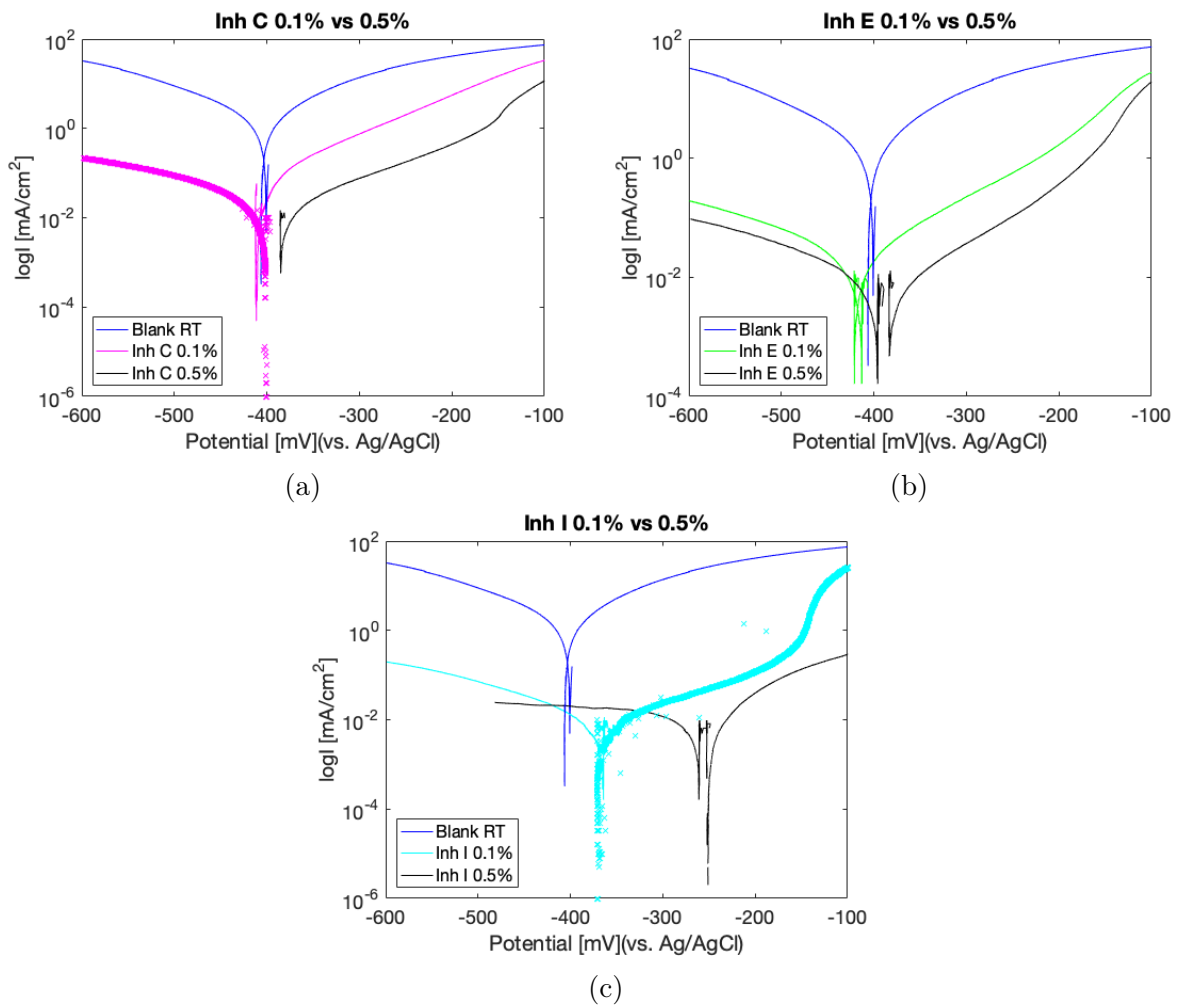


Figure 33: Comparison of polarization curves of each inhibitors with different concentrations in 15 % HCl at room temperature without CO₂.

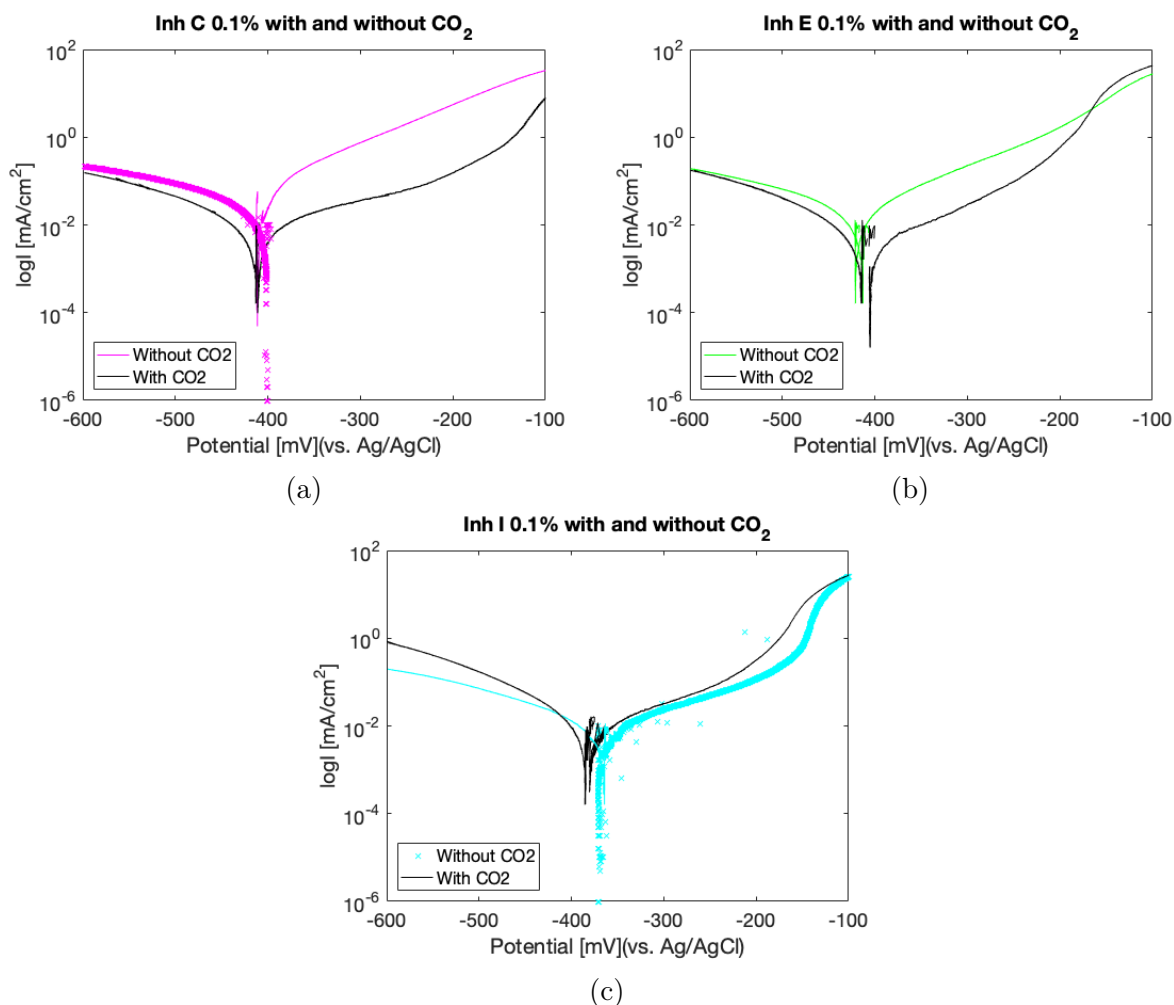


Figure 34: Comparison of polarization curves of each inhibitors (0.1 vol.%) with and without CO₂ in 15% HCl at room temperature.

Potentiodynamic polarization curves for C1020 in carbon dioxide saturated HCl solution are illustrated in Figure 34. Three inhibitors with the highest IE values resulting from the weight loss experiments were selected for this experiment. In the presence of carbon dioxide Inhibitor C and Inhibitor E show reduced current density of the steel compared to experiments without CO₂. However, the cathodic reaction was not suppressed as much as the anodic reaction. Inhibitor I, on the other hand, displays gentle increase of cathodic and anodic corrosion current density in the presence of CO₂. Tafel polarization curves of different inhibitors in carbon dioxide saturated HCl solution are plotted together in the Figure 35. Inhibitor C and Inhibitor E show almost the same cathodic polarization behaviour, which suggests that their protection mechanisms are similar [48]. The Inhibitor C has the lowest current density.

Figure 36 displays polarization curves of inhibitors with 0.1% at 50°C and all inhibitors have lower anodic and cathodic current density than the blank experiment, which was also proven in the experiment at room temperature (see Figure 31). Among all tested inhibitors, Inhibitor I has the lowest current densities, which is the same at the room temperature without CO₂.

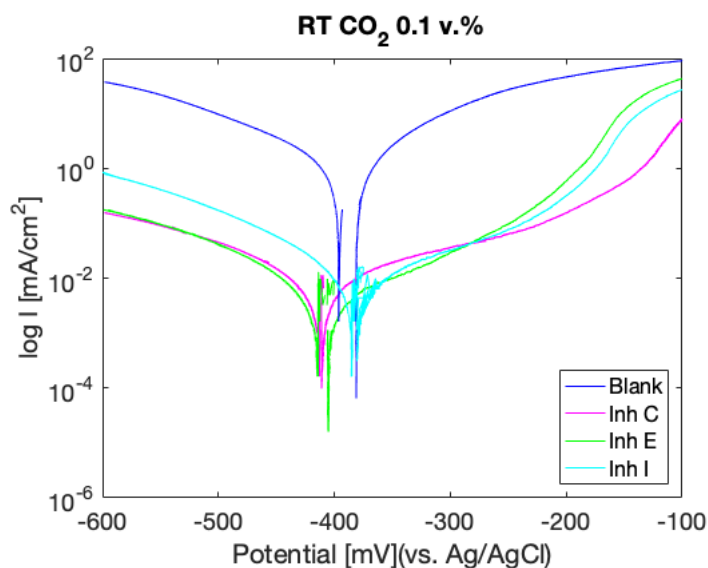


Figure 35: Tafel polarization curves of different inhibitors with 0.1 vol.% measured at room temperature, while carbon dioxide gas was purged into the electrolyte.

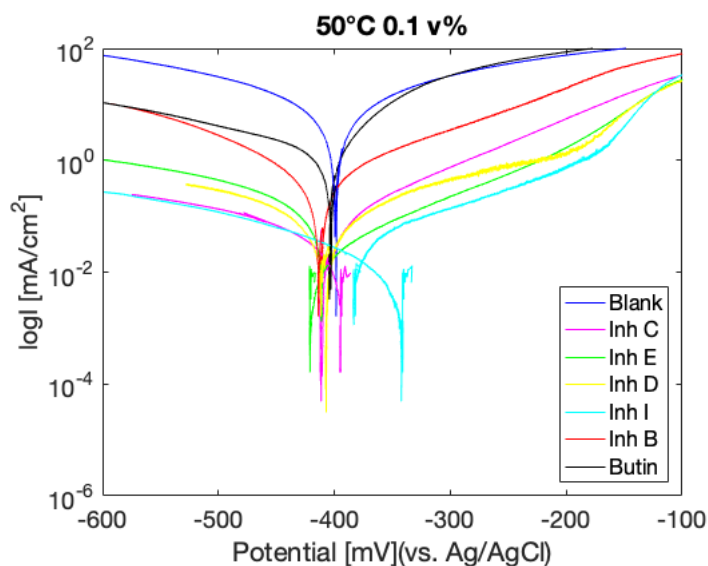


Figure 36: Tafel polarization curves of different inhibitors with 0.1 vol.% measured at 50°C without CO₂.

4.3 Open circuit potential (OCP)

Observing OCP as a function of time counts as an important method to detect initiation of corrosion [49]. By monitoring change of OCP value a simple statement about the state of the film on the metal can be made. Furthermore, shift of OCP can mean either one side reaction was heightened or the other lowered. If the potential is steady, then there is no change in film. The Figure 37 illustrates the course of potential as a function of time. The addition of Inhibitor E at approx. 300 seconds induces sharp rise of OCP, which drops rapidly and slowly rises again. After some time decrease of the potential becomes steady, which indicates the formation of inhibitor film on the sample was still ongoing. The continuous growth of the film could be also seen in the impedance data (Figure 38). It shows three consecutive measurements, black curve being the first measurement and the blue the last. The first measurement was carried out 55 minutes after the addition of inhibitor, the second measurement 65 minutes and the third measurement 75 minutes. The radius of the semicircle grows in the Nyquist plot and similarly the increase of resistance can be found in the Bode plot.

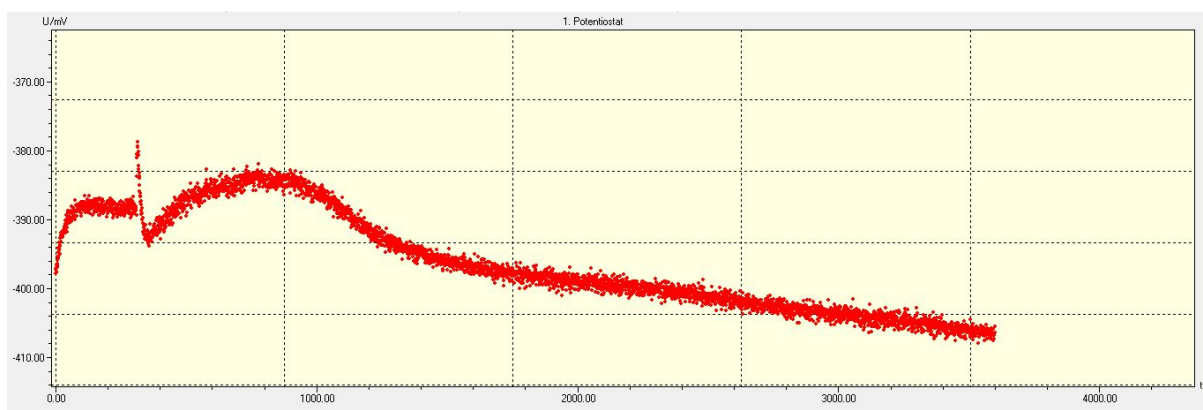


Figure 37: OCP curve in 0.1% Inhibitor E at 50°C.

Inhibitor I, on the other hand, shows more or less steady potential after 2400 seconds, from which also intact film formation can be presumed (see Figure 39). The Figure 40 shows the impedance measurements, which were executed three times consequently with one single pair of coupons. The first measurement was carried out 55 minutes after the addition of inhibitor, the second measurement 65 minutes and the third measurement 75 minutes. The impedance curves in the Nyquist plot are spiky, which are not easy to interpret, however, the Bode plot (Figure 40b) has fairly smooth lines, from which the steady protection of metal is proved. Furthermore, when the inhibitor was added, the OCP shifted towards more positive value which means the surface became nobler and the passive protective film is formed on the surface [52]. Figures 41, 42 and 43 are

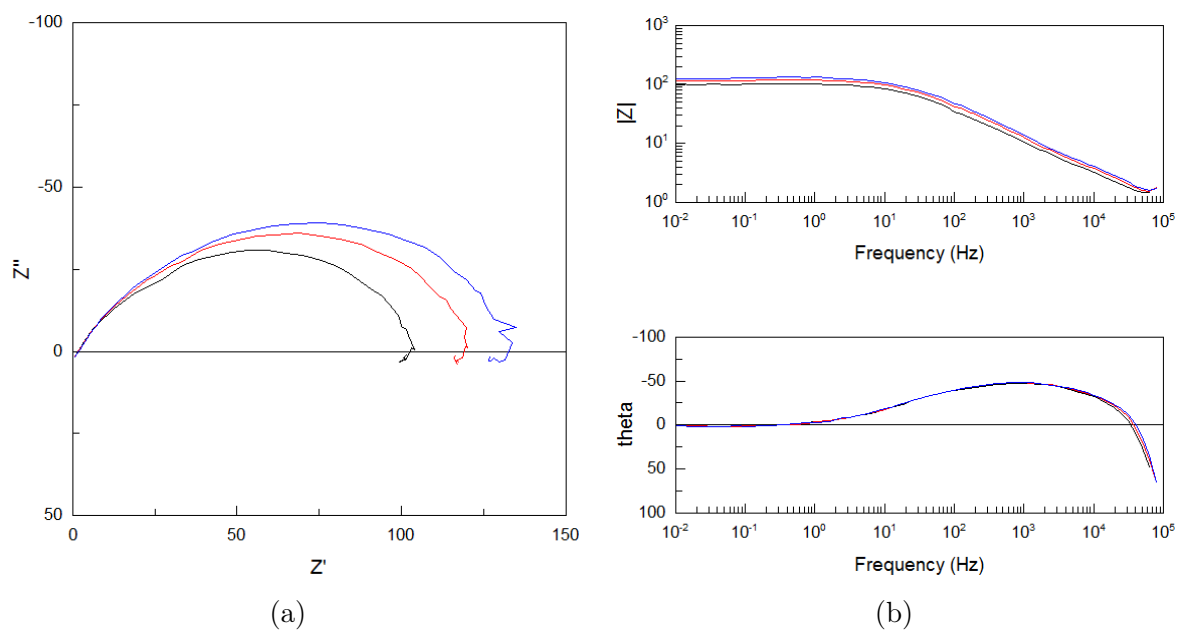


Figure 38: (a) Nyquist plot and (b) Bode plot of Inhibitor E at 50°C with 0.1% concentration.

OCP plots of Inhibitor E, but in different experimental conditions. Further OCP plots are presented in appendix, which is the measure whether EIS measurements were carried out in the quasi-steady state.

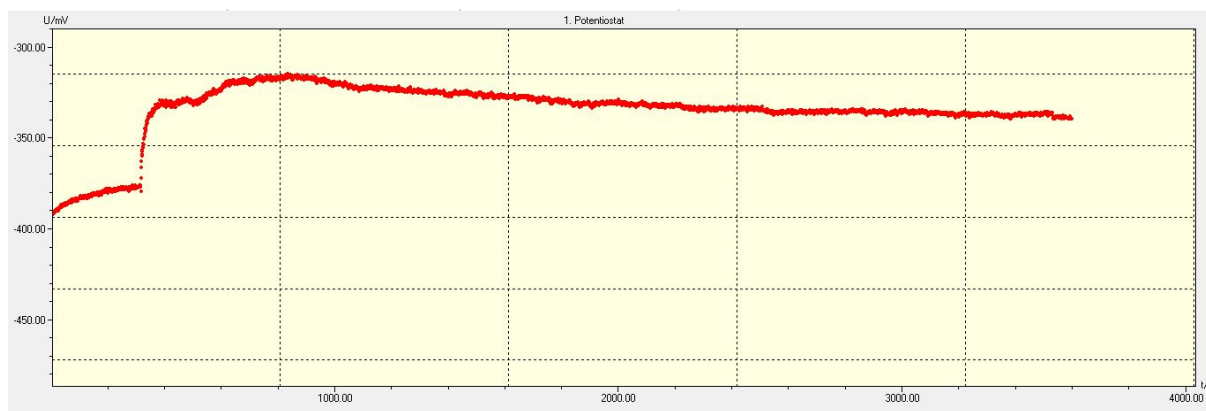


Figure 39: OCP curve in 0.1% Inhibitor I at RT.

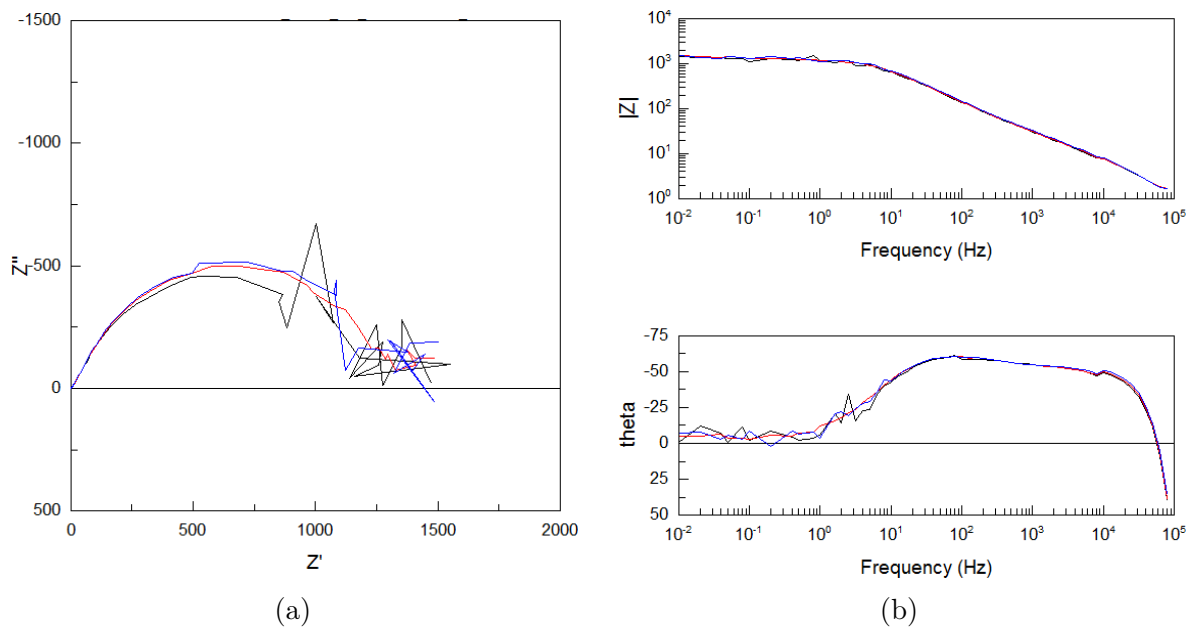


Figure 40: Nyquist plot and Bode plot of Inhibitor I at room temperature with 0.1% concentration.

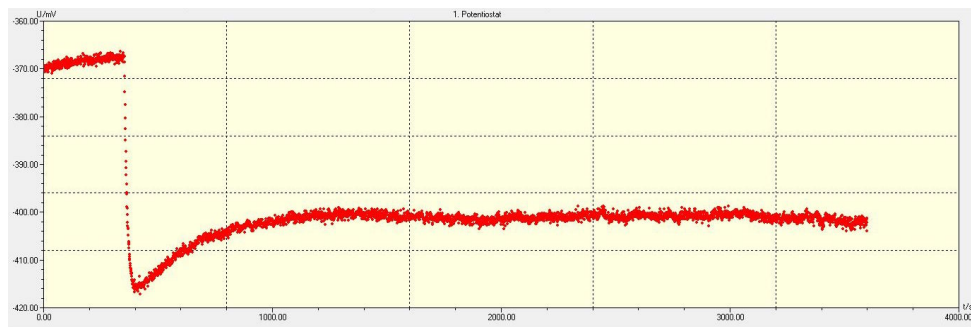


Figure 41: OCP curve in 0.1% Inhibitor E at RT in CO_2 saturated hydrochloric acid solution.

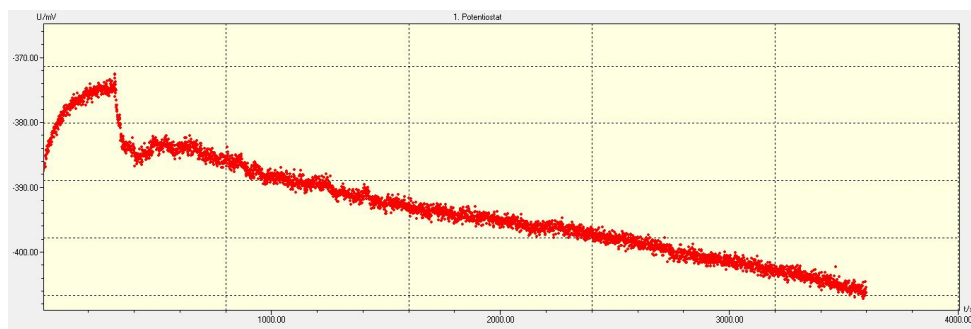


Figure 42: OCP curve in 0.1% Inhibitor E at RT without CO_2 .

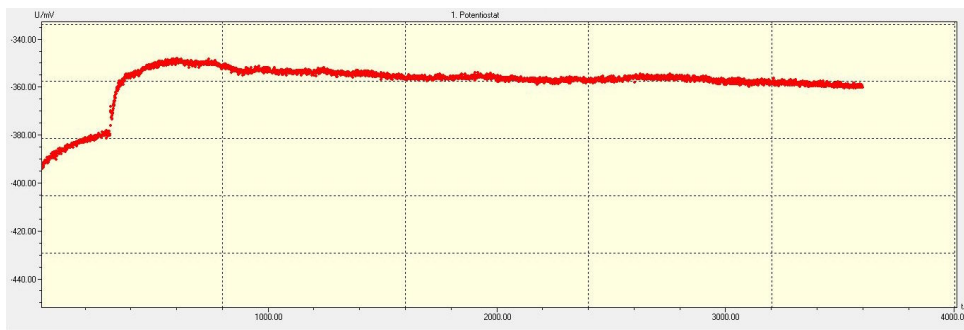


Figure 43: OCP curve in 0.5% Inhibitor E at RT without CO₂.

4.4 Electrochemical impedance spectroscopy measurements

Electrochemical impedance spectroscopy was used in order to investigate the corrosion behaviour of steel in the presence and absence of inhibitors in diluted hydrochloric acid solution. The equivalent electric circuits in Figure 44 were used to fit the impedance data. R_{el} [Ω] in the model represents the solution resistance, the summation of the R_0 , R_1 and R_2 (and R_3) represents polarization resistance (R_p [Ω]) and CPE a constant phase element. The models in Figure 44a and 44b were used for data with and without an inductive loop respectively. By using these models excellent fits were achieved as it can be seen in the Figure 45.

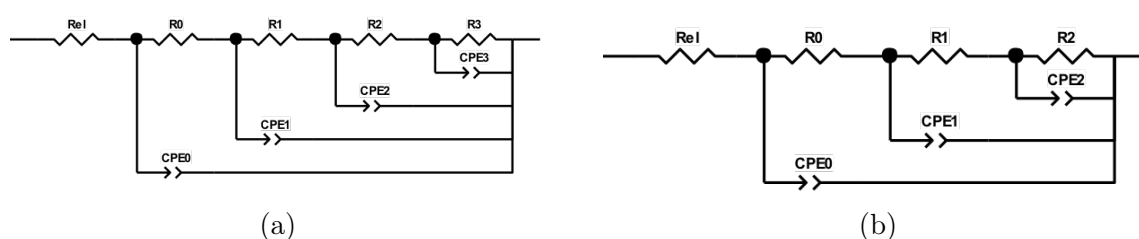


Figure 44: Equivalent electric circuit model used to fit impedance data.

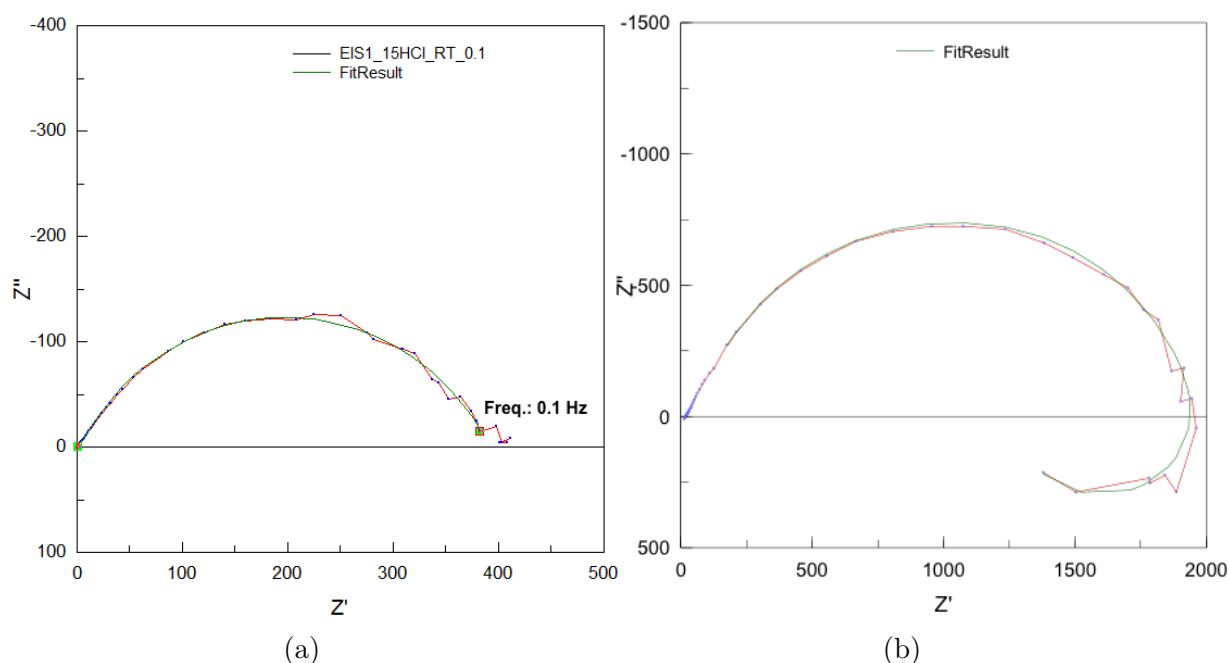


Figure 45: Fitted impedance data of (a) Inhibitor D at room temperature (b) Inhibitor I at room temperature with 0.5% concentration without CO_2 .

The inhibition efficiency (or protection rate) was calculated as follows:

$$IE = \left(\frac{R_p - R_p^0}{R_p} \right) * 100 \quad (23)$$

As it was discussed before, R_p was calculated according to the model as follows:

$$R_p = R_0 + R_1 + R_2 (+R_3) \quad (24)$$

R_p and R_p^0 are the transfer resistance with and without the inhibitor (blank value), respectively. As R_p^0 five blank values were chosen for each set of experiments and an average was calculated and the average value was used to calculate the inhibitor efficiency: For example five blank values at room temperature without CO_2 were taken and this average was used as R_p^0 and IE of inhibitors at this exact condition was calculated. Taking the averaged R_p^0 values is justified, as the blank values of all individual measurements are more or less the same within the identical experimental condition (see Figure 46).

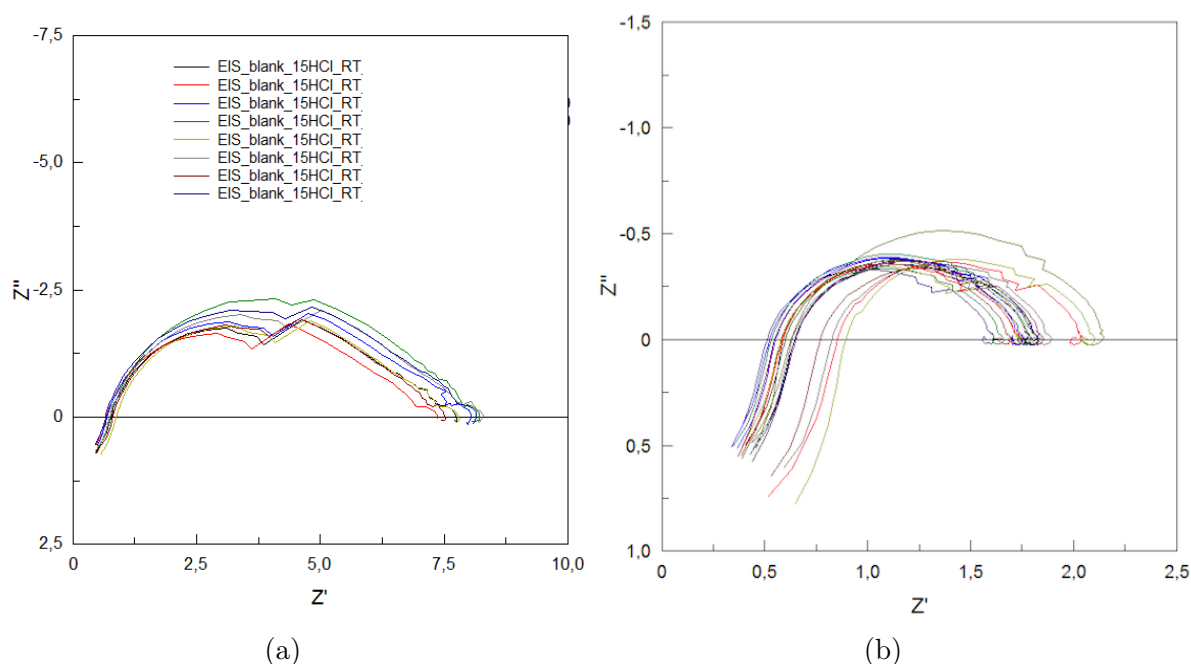


Figure 46: Nyquist plot for C1020 steel in 15% HCl solutions without CO_2 at room temperature (a) and $50^\circ C$ (b).

The Nyquist plot for C1020 alloy in 15% HCl solution at room temperature and at $50^\circ C$ is presented in the Figure 47a and 47b. As it can be seen, Inhibitor I has the largest radius and Butindiol the smallest, which indicates that they protect the metal surface the best and the least, respectively. It is also notable that the radius decreases as the

temperature is set higher. At the room temperature, zigzag type pattern was observed

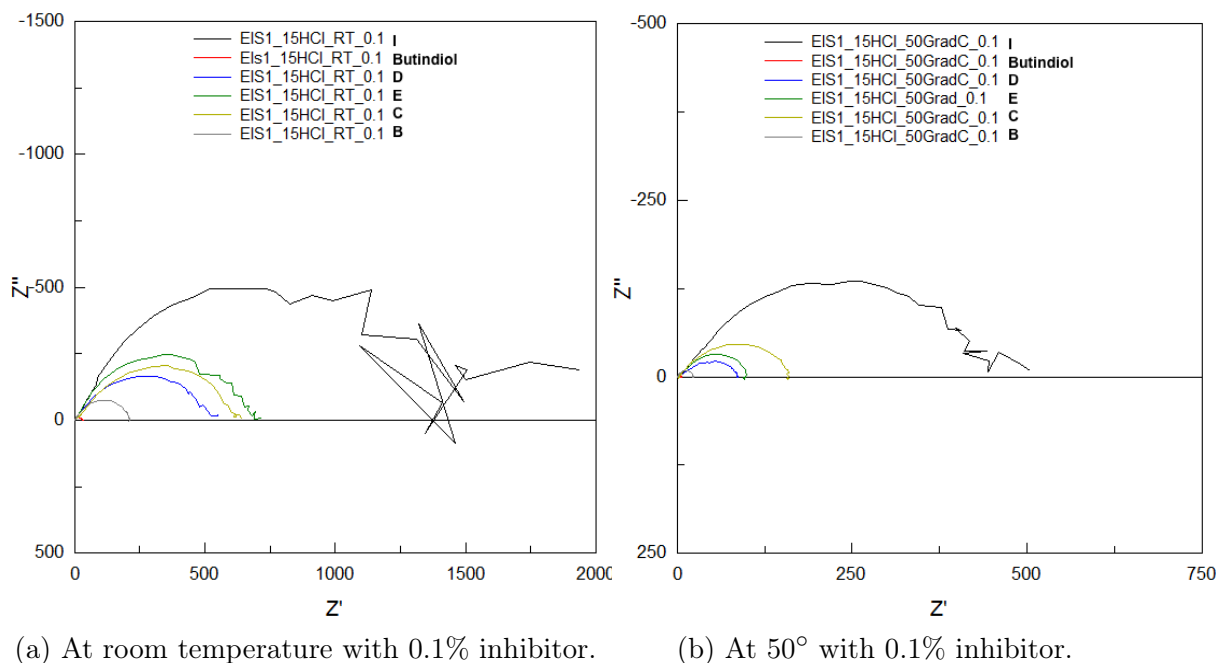


Figure 47: Nyquist plot for C1020 steel in 15% HCl solutions with 0.1% inhibitor at different experimental conditions.

mainly on the curves with the two largest arc radius (Inhibitor E and I). The same trend was shown also when the measurement was executed at 50°C. Interestingly, the frequency (and resistance) at which the round arc of a semicircle stops varies depending on the inhibitor. For instance, it was 3.976 Hz (480Ω) and 5 Hz (825 Ω) for Inhibitor E and I at room temperature, respectively (shown in the Figure 47a). At the elevated temperature shown in Figure 47b the frequency lowers to 2 Hz where the noise starts showing (in case of Inhibitor I). From this it can be deduced that this atypical pattern is not solely caused by high Z' . One possible explanation for this zigzag pattern is the instability of the system, i.e. the system had not reached the quasi-steady state during the measurement. Thus, OCP measurements of Inhibitor B and I are compared, as OCP measurement is a measure of the stability of a system (see Figure 48 and 49). For the comparison Inhibitor B was chosen as it showed smooth curve in Nyquist plot in Figure 50. OCP measurement of Inhibitor B suggests (Figure 49), that the system had not reached the quasi steady state yet as the potential varies. On the other hand, the open circuit potential of Inhibitor I did not show much change compare to Inhibitor B, displaying quasi steady state .

Another factor which may have caused the zigzag pattern is the potentiostat itself. As the

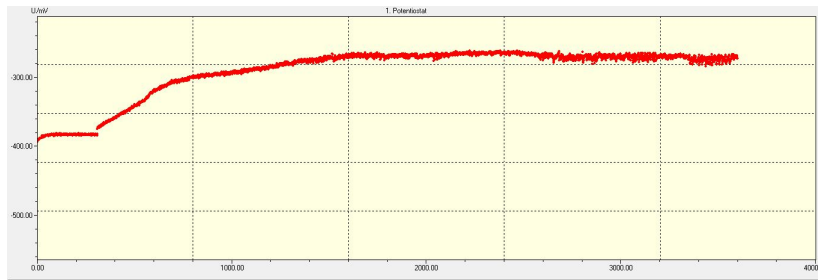


Figure 48: OCP measurement of Inhibitor I at 50°C with 0.1% inhibitor.

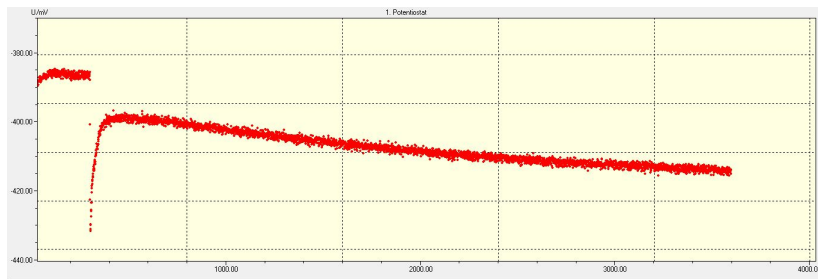


Figure 49: OCP measurement of Inhibitor B at 50°C with 0.1% inhibitor.

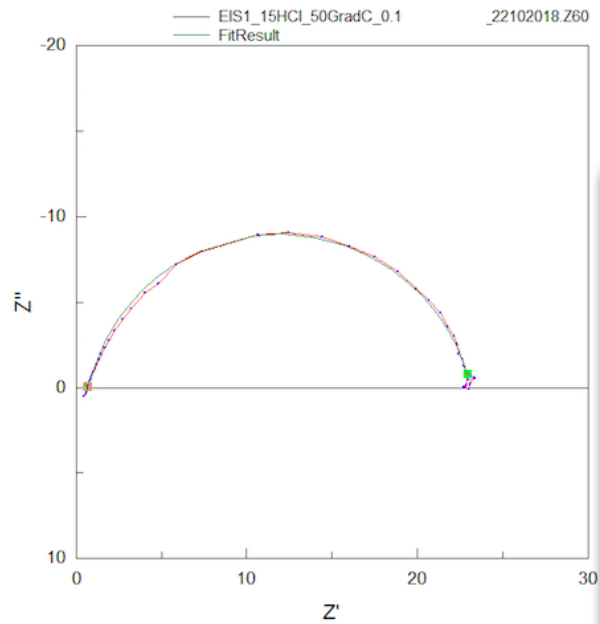


Figure 50: Nyquist plot of Inhibitor B at 50°C with 0.1% inhibitor.

flaw in the instrument was considered, a test was run with a dummy cell. The identical measurement was run with a different instrument in TU Wien in order to compare the results and it is represented in the Figure 51. Similar to the measurements with inhibitors zigzag pattern was shown as the resistance exceeds 750 Ω (red line). The measurement run at TU with a different instrument, on the other hand, shows an intact semi circle.

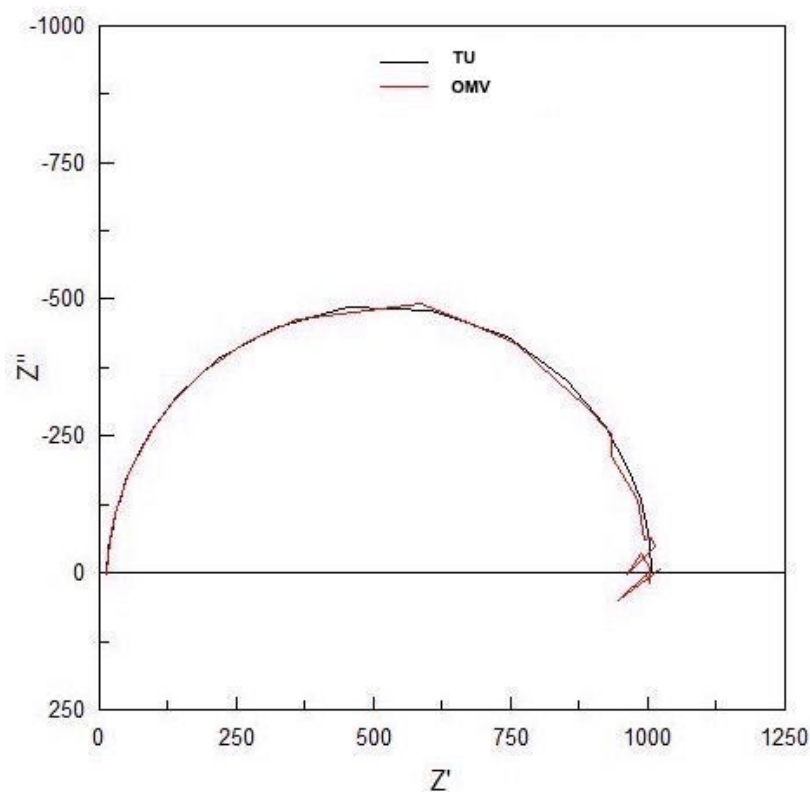


Figure 51: Nyquist plot of a dummy cell measured with two different instruments.

From this comparison, it can be concluded that the instrument does contribute to the highly fluctuating resistance values to a certain degree.

The inhibitor efficiency was calculated and is shown in the Table 7.

Inhibitor	IE [%]	
	RT	50°C
Inhibitor B	96.73 ± 0.1	94.85 ± 1.15
Inhibitor C	98.85 ± 0.04	99.43 ± 0.20
Inhibitor D	98.48 ± 0.05	98.95 ± 0.29
Inhibitor E	98.97 ± 0.03	99.00 ± 0.24
Inhibitor I	99.52 ± 0.02	99.68 ± 0.15
Butindiol	76.99 ± 0.76	56.62 ± 4.92

Table 7: Inhibitor efficiency of inhibitors (0.1 vol.%) measured with EIS at room temperature and 50°C.

At room temperature and 50°C butindiol has the lowest IE. This was expected as butindiol is a single substance that was used diluted and is not a sophisticated mixture of interacting compounds like commercial acid corrosion inhibitor. Other than Inhibitor B,

all inhibitors have comparable IE, ranging between 98% and 99%. Lower IE of Inhibitor B was not a surprise, as it was designed for less corrosive environment than HCl. However, IE values calculated from EIS are not considered as a optimal mean of comparing the performance of inhibitors, since the R_p of Inhibitor D is approximately one third of Inhibitor I at both temperatures and the IE value difference is only 1%. Therefore, another parameter normalized polarization resistance, R_{pn} was additionally calculated by using this equation:

$$R_{pn} = \frac{R_p \cdot A}{2}, \quad (25)$$

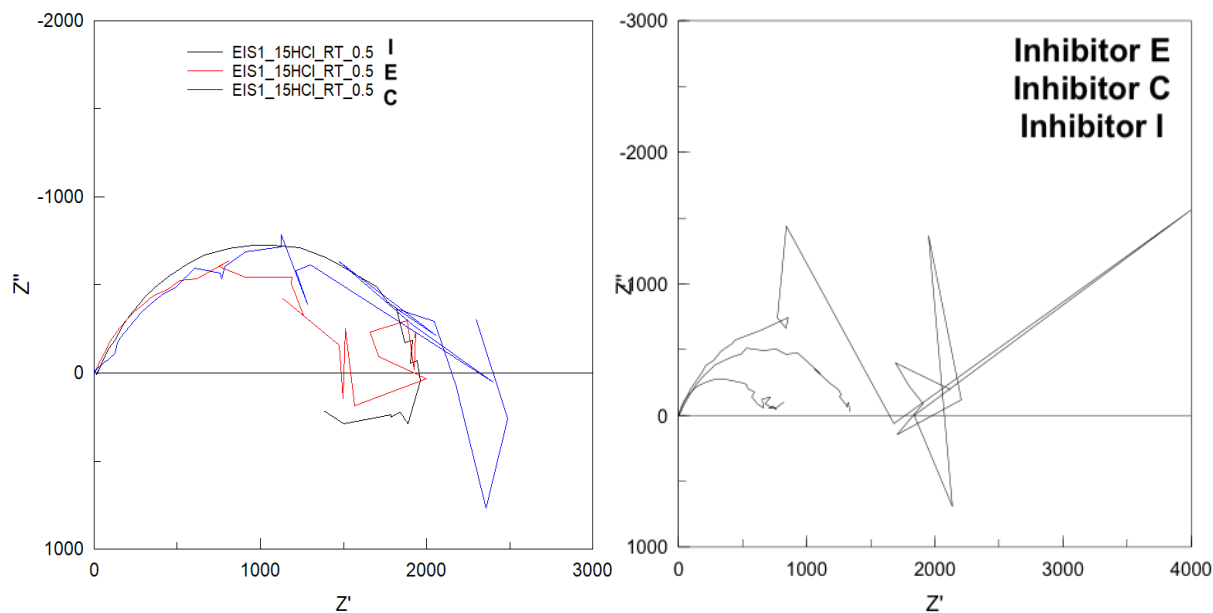
whereas A stands for the surface area of the sample (3.76 cm^2). The R_{pn} values are shown in the table 8. By listing the normalized polarization resistance, the effect of increasing temperature can be clarified. At the elevated temperature lower R_{pn} was observed for all the used chemicals and the normalized polarization resistance of Inhibitor C and I are reduced by around 3.5. R_{pn} of other inhibitors and butindiol were decreased by up to factor 10.

Inhibitor	$R_{pn} [\Omega \text{ cm}^2]$	
	RT	50°C
Inhibitor B	395.71 ± 15.44	39.67 ± 2.34
Inhibitor C	1123.45 ± 46.52	301.99 ± 128.93
Inhibitor D	869.09 ± 136.79	199.33 ± 34.59
Inhibitor E	1248.68 ± 29.60	205.78 ± 20.50
Inhibitor I	2663.01 ± 49.90	738.05 ± 254.30
Butindiol	56.08 ± 0.64	9.21 ± 0.47

Table 8: Normalized polarization resistance of inhibitors (0.1 vol.%) measured with EIS at room temperature and 50°C.

The EIS measurements were executed at room temperature with 0.5% inhibitor without CO_2 and 0.1% with CO_2 . These spectra are presented in the Figure 52. Similar to the Figure 47, zigzag patterns can be found also in these experiments. The black curve in the Figure 52a (Inhibitor I) shows clearly two impedance loops. The first loop at high frequency range is a polarization resistance loop and the second loop at low frequency is an inductive loop. It is challenging to characterize how many loops the impedance response consists of due to the severe fluctuation within the other two curves (Inhibitor C and E in Figure 52a). The same applies to the impedance response of Inhibitor E and

I in the Figure 52b, even though the atypical pattern may be not too severe in case of Inhibitor I. Tables from 9 to 12 show that the Inhibitor I has the highest IE and R_{pn} in carbon dioxide saturated HCl at room temperature with 0.5 vol.%, however without the presence of CO_2 and the concentration was reduced to 0.1 vol.%, then the Inhibitor E shows the best result.



(a) At room temperature with 0.5% inhibitor without CO_2 . (b) At room temperature with 0.1% inhibitor and CO_2

Figure 52: Nyquist plot for C1020 steel in 15% HCl solutions in different experimental conditions.

Inhibitor	IE [%] RT (0.5 vol.%)
Inhibitor C	98.98
Inhibitor E	98.90 ± 0.01
Inhibitor I	99.63 ± 0.01

Table 9: Protection rate of inhibitors (0.5 vol.%) measured with EIS at room temperature.

Inhibitor	R_{pn} [Ω cm ²] RT (0.5 vol.%)
Inhibitor C	1169.98
Inhibitor E	2928.13 \pm 250.78
Inhibitor I	3477.41 \pm 146.77

Table 10: Normalized polarization resistance of inhibitors (0.5 vol.%) measured with EIS at room temperature.

Inhibitor	IE [%] RT & CO ₂ (0.1 vol.%)
Inhibitor C	99.44 \pm 0.14
Inhibitor E	99.72 \pm 0.07
Inhibitor I	99.05 \pm 0.24

Table 11: Protection rate of inhibitors (0.1 vol.%) measured with EIS at room temperature with CO₂ bubbling.

Inhibitor	R_{pn} [Ω cm ²] RT & CO ₂ (0.1 vol.%)
Inhibitor C	2410.00 \pm 133.27
Inhibitor E	4758.30 \pm 207.51
Inhibitor I	1414.13 \pm 92.94

Table 12: Normalized polarization resistance of inhibitors (0.1 vol.%) measured with EIS at room temperature with CO₂ bubbling.

4.4.1 Repeatability- 0.1% inhibitor at room temperature without CO₂

The Figure 53 - 58 shows the Nyquist plots of EIS data measured at room temperature with 0.1% inhibitor concentration. The inhibitors were added with a pipette directly to the electrolyte without being diluted beforehand. Two independent experiment results (two semi-circles) are displayed in one plot and compared. By two independent experiments, two different pair of metal coupons and new electrolyte are meant. Despite the fact that none of the curves are exactly reproducible with any of the used chemicals, it is remarkable that the curves for each inhibitor take similar shape. Furthermore, apart from Inhibitor D the radii of curves lie in a comparable range.

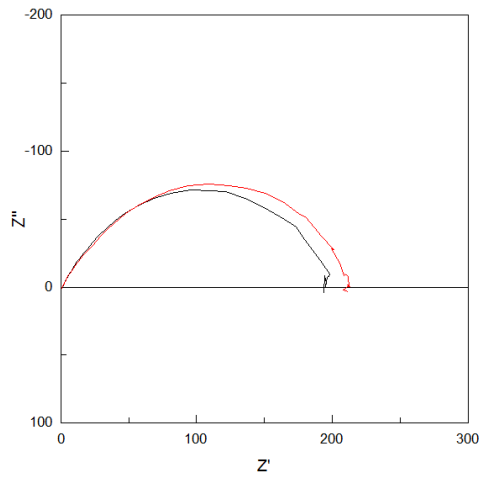


Figure 53: Inhibitor B at room temperature without CO₂ with 0.1% concentration.

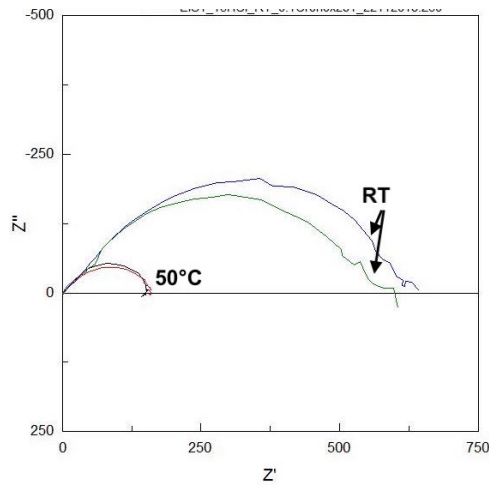


Figure 54: Inhibitor C at room temperature and 50°C without CO₂ with 0.1% concentration.

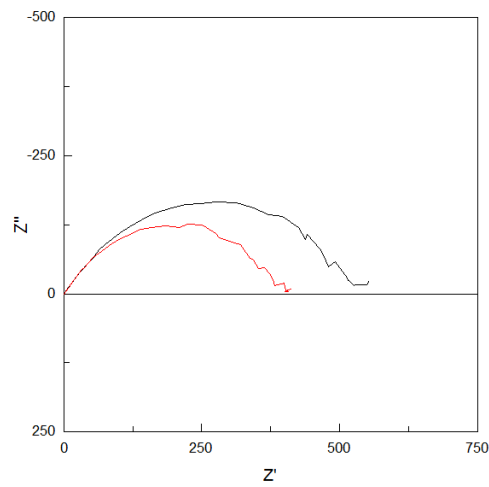


Figure 55: Inhibitor D at room temperature without CO₂ with 0.1% concentration.

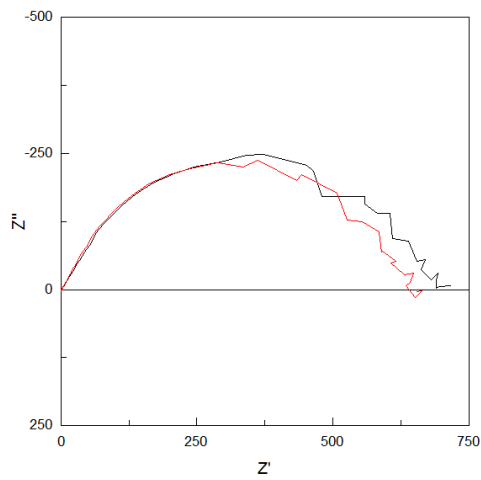


Figure 56: Inhibitor E at room temperature without CO₂ with 0.1% concentration.

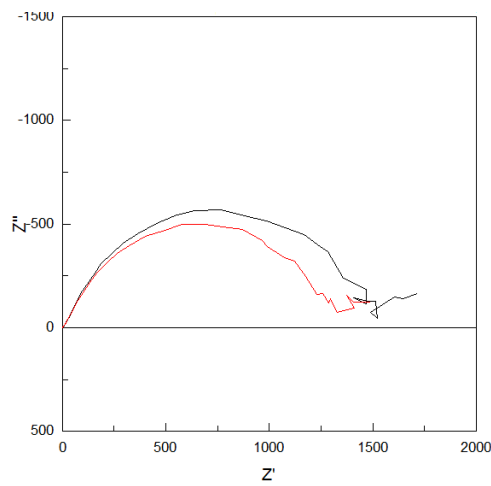


Figure 57: Inhibitor I at room temperature without CO₂ with 0.1% concentration.

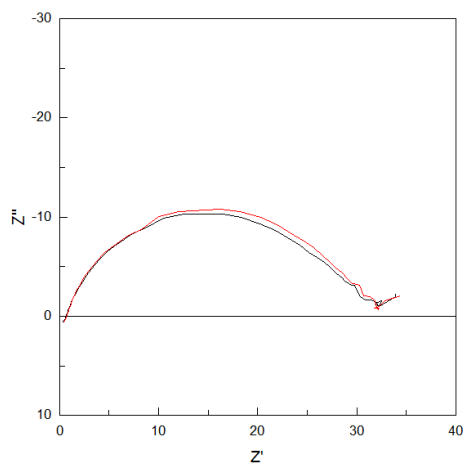


Figure 58: Butindiol at room temperature without CO₂ with 0.1% concentration.

4.4.2 Repeatability- 0.1% inhibitor at 50°C without CO₂.

The Figure 59 - 64 show the EIS data of measurements carried out at 50°C with 0.1% inhibitor concentration. Experiments were repeated at least twice independently and the results are plotted in one Nyquist diagram. Similar to the experiments at room temperature butindiol, Inhibitor B and C showed quite good reproducibility with comparable shape of curves and radii.

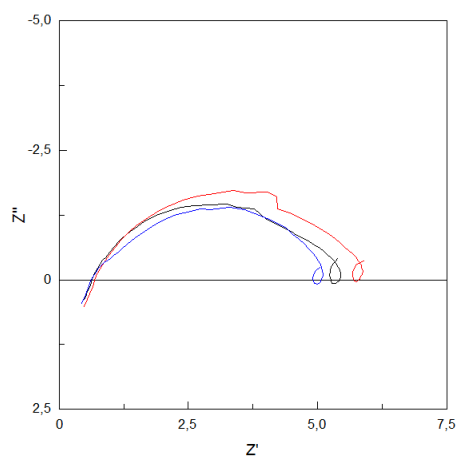


Figure 59: Butindiol at 50°C without CO₂ with 0.1% concentration.

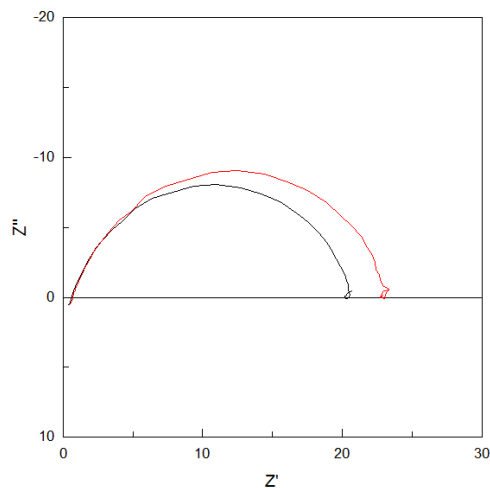


Figure 60: Inhibitor B at 50°C without CO₂ with 0.1% concentration.

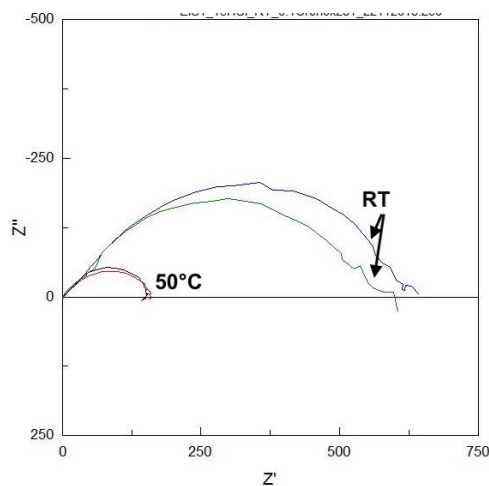


Figure 61: Inhibitor C at 50°C without CO₂ with 0.1% concentration.

Even at room temperature, when other inhibitors proved acceptable repeatability, Inhibitor D showed otherwise. With no surprise EIS data of Inhibitor D was not reproduced at elevated temperature. Impedance of Inhibitor E was measured also five times, however

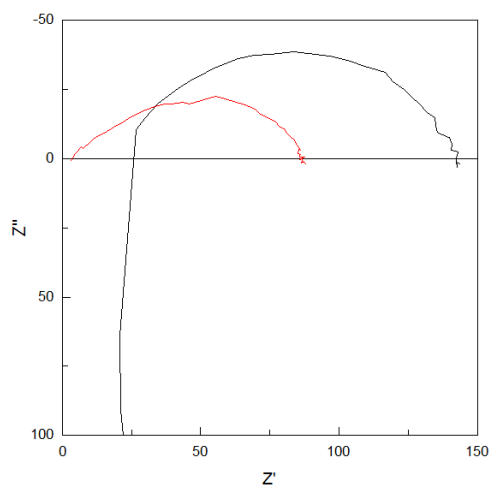


Figure 62: Inhibitor D at 50°C without CO₂ with 0.1% concentration.

its reproducibility proves to be better than Inhibitor I as the Z' range "only" between 97 and 126 Ω .

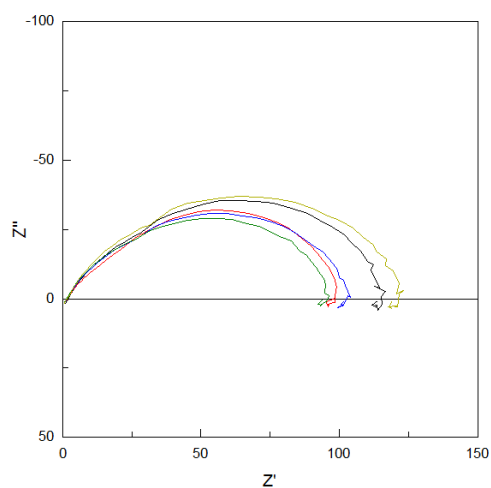


Figure 63: Inhibitor E at 50°C without CO₂ with 0.1% concentration.

Experiment with Inhibitor I was repeated five times since each curve had different Z' from the others (see Figure 64). With the software fitted radii of curves range between 198 and 580 Ω .

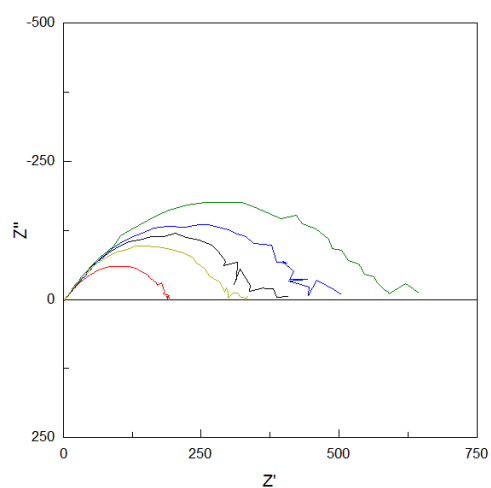


Figure 64: Inhibitor I at 50°C without CO₂ with 0.1% concentration.

4.4.3 Repeatability- 0.1% inhibitor at room temperature with CO₂.

Impedance was measured twice independently for Inhibitor E and I and the result is displayed on one plot. As it can be seen in Figure 65 and 66, statements about the repeatability is difficult to make due to the severe zigzag pattern.

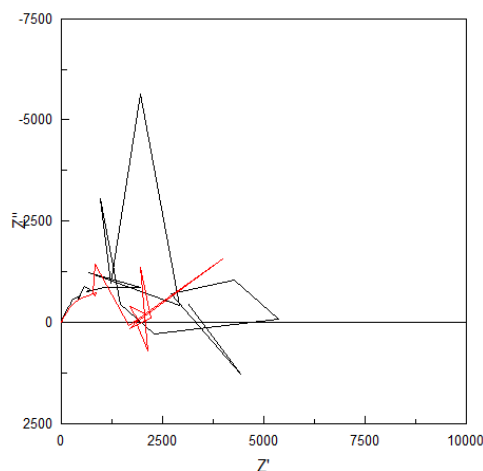


Figure 65: Inhibitor E at room temperature with CO₂ with 0.1% concentration.

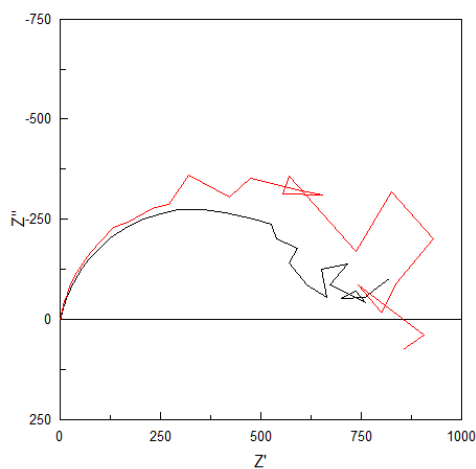


Figure 66: Inhibitor I at room temperature with CO₂ with 0.1% concentration.

Inhibitor C was measured twice as well (see Figure 67). Compared to two other inhibitors (Inhibitor E and I) the severity of zigzag pattern is visibly toned down.

4.4.4 Repeatability- 0.5% inhibitor at room temperature without CO₂.

The Figure 68 shows two independent measurements (two different pairs of coupons and new electrolyte) with Inhibitor I and each measurement was repeated three times with

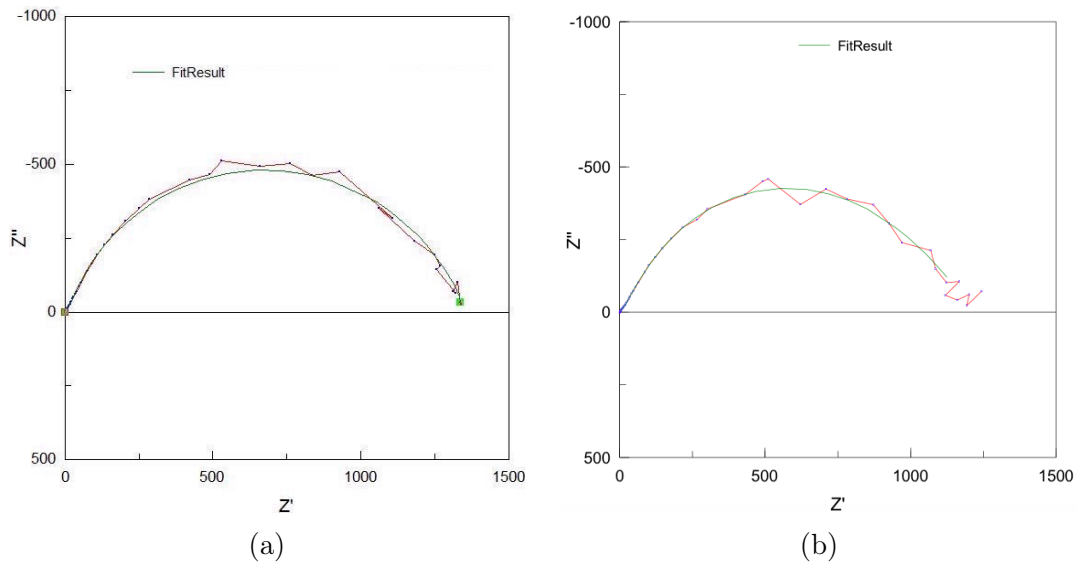


Figure 67: Two independent measurements of Inhibitor C at room temperature with CO₂ with 0.1% concentration.

the same pair of coupons. It can be noticed that both figures visibly differ from each other: Figure 68a has clearly inductive loops, whereas they are not as clearly noticeable in the Figure 68b. In case of Inhibitor E the EIS data cannot be reproduced due to the

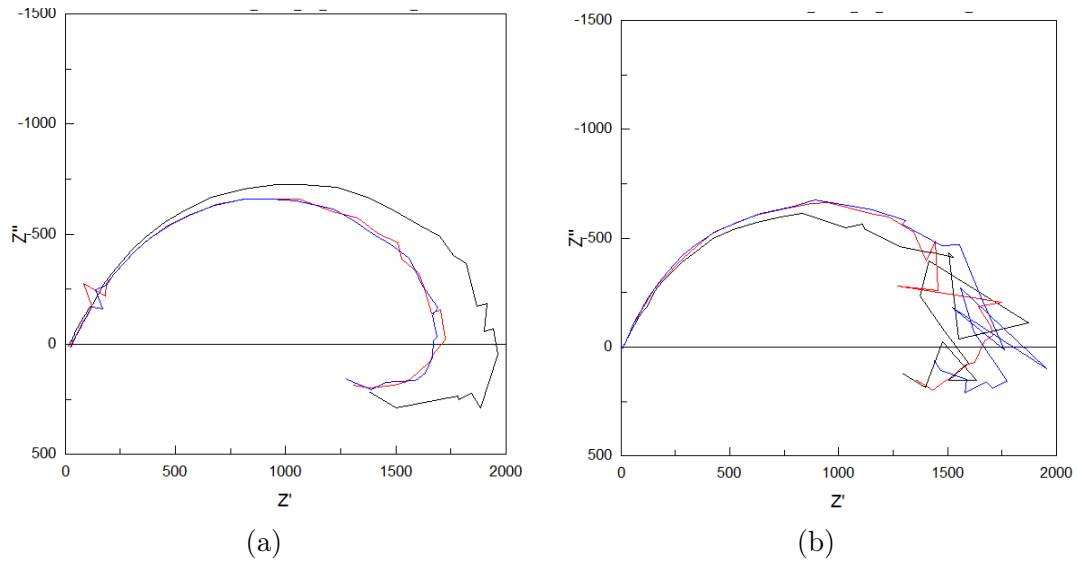


Figure 68: Two independent measurements of Inhibitor I at room temperature without CO₂ with 0.5% concentration.

rough semi-circle as it is shown in the Figure 69.

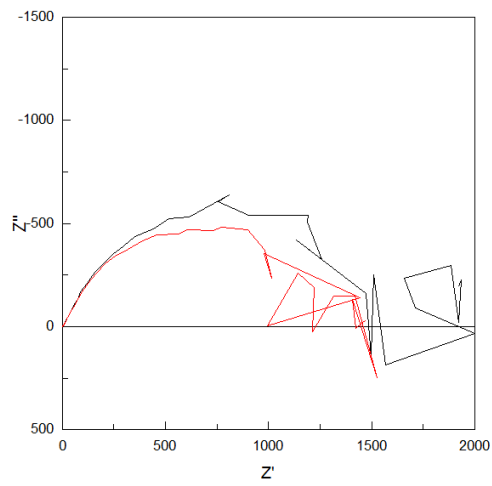


Figure 69: Inhibitor E at room temperature without CO₂ with 0.5 % concentration.

4.5 Surface

Beside the impedance curves, it was also of interest to have a closer look on the surface beneath the acrylic resin (see Figure 70). By comparing this surface with the surface which is exposed directly to the 15% HCl, a conclusion can be drawn, whether the acrylic resin was liquid-tight, so that no crevice corrosion took place and the sample was not attacked by the acid solution. This is crucial as the normalized polarization resistance is direct by proportional to the exposed surface area. The metal coupons after the polarization experiments were taken and treated as it is described in the experimental part 3.3. The Figure 71 is a picture of the sample embedded in black resin, whereas the metal sample is shown as white and the resin grey. The darker grey area within the concave boundary is the acrylic resin which was applied on the coupons during the preparation of samples.

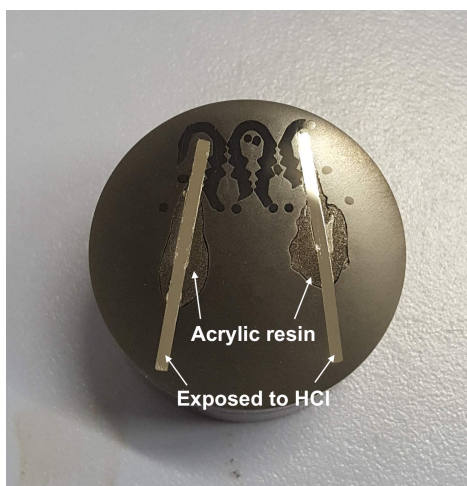
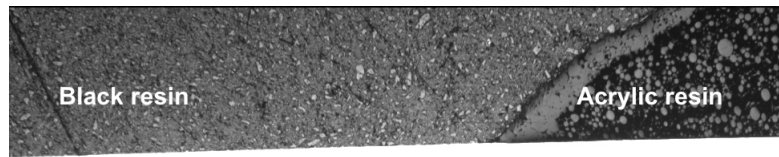


Figure 70: Metal coupon and acrylic resin embedded in the black resin.

The Figure 72 shows the metal surface which was directly touching the acid solution. The only difference in these two Figures is the brightness, which was set when the pictures were taken.

The surface underneath the acrylic resin is depicted in the Figure 73a and 73b. Also here the only difference between these two pictures is the brightness.

As expected the metal surface in Figure 72 is bumpier than in Figure 73 due to the corrosion in the acid media. The metal protected by the acrylic resin shows smoother surface, from which it can be confirmed that the HCl solution does not creep in through the acrylic resin and affect the results of electric impedance spectroscopy. In other words, no crevice corrosion took place.



Metal sample



Figure 71: Metal coupon under the microscope after finishing experiments. The coupon is shown as white, lighter grey part is the resin for embedding and the darker grey area is the acrylic resin.

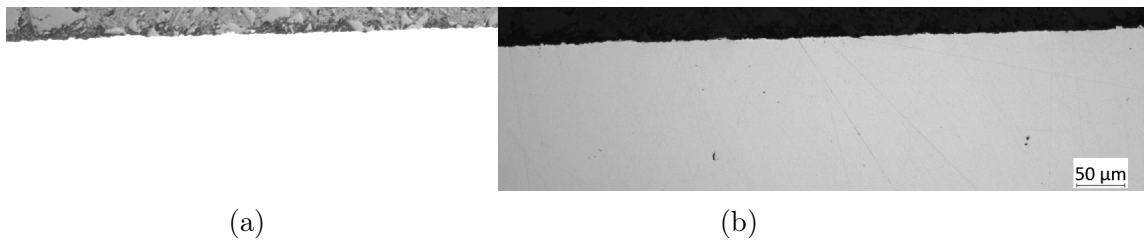


Figure 72: Part of the metal coupon, which was dipped in the hydrochloric acid. The left picture was better lit than the right one.

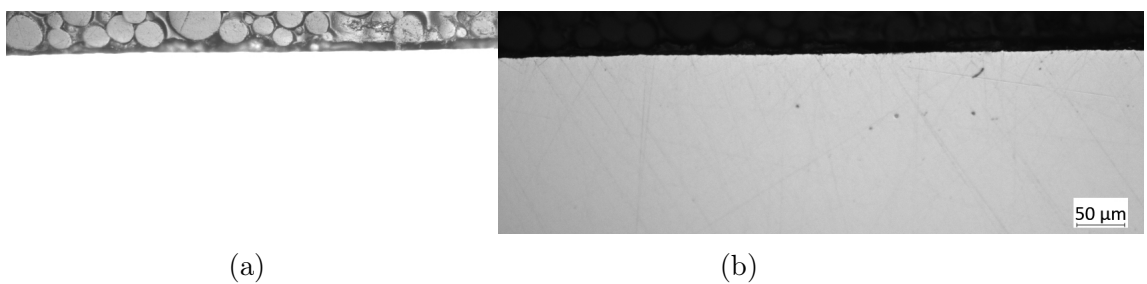


Figure 73: Part of a metal coupon, which did not have any contact with the hydrochloric acid. The left picture was better lit than the right one.

4.6 Experimental parameters

Apart from measuring impedance of inhibitors at different conditions, improving the reproducibility was a part of this work. This was realized by changing a few experimental

parameters.

4.6.1 Adding inhibitors

One of the first parameters changed was the way of adding the inhibitors. Originally the inhibitors were diluted in 15% HCl solution 1 : 10. However, the challenge was to achieve a homogeneous mixture of inhibitors and HCl solution. Figure 74 shows Inhibitor E in HCl solution a day after the mixing and tiny droplets on the wall were observed due to the lack of solubility. Inhibitor D showed also low solubility in HCl solution (see Figure 75). By the time when this picture was taken, this solution had not been stirred for two days since the day of dilution.

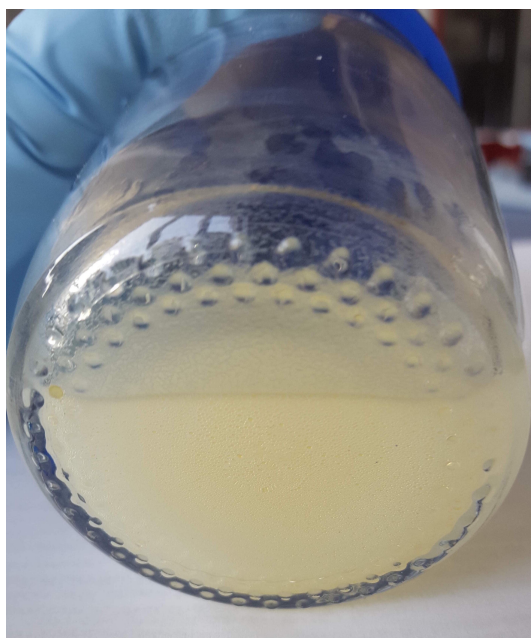


Figure 74: Inhibitor E mixed into hydrochloric acid.

According to the data sheet of the inhibitors mentioned above, they consist of higher alcohols. In order to achieve more homogeneous solution without any phase separation, which was observed with 15% HCl, methanol was taken as a diluent. As it can be seen in the Figure 76, despite changing the diluent to methanol, small droplets on the wall of the container were still visible.

Finally, it was considered to be the best option to add the inhibitor directly using a pipette. However, great care must be taken, that the tip does not touch the electrolyte, as the viscosity of inhibitors is high and tend to remain on the outer side of tips. This would lead to unintended extra amount of inhibitors.



Figure 75: Inhibitor D mixed into hydrochloric acid.

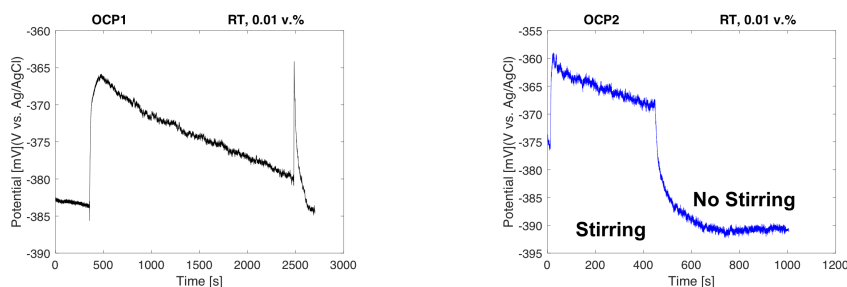


Figure 76: Inhibitor D mixed into methanol.

4.6.2 OCP measurement

The duration of open circuit measurement was changed from 45 minutes to 60 minutes in order to give the system more time to reach the quasi steady state. Beside the extension of the length of OCP measurement, the solution was stirred with a magnet stirrer during the OCP measurement. The two subfigures 77a and 77b show the measurements, which

are executed one after the other. During the first measurement (Figure 77a) the system was not stirred, whereas in the second measurement the system was stirred first and stopped (Figure 77b). The increase of potential around 400 seconds in the Figure 77a is caused by the addition of the inhibitor and the potential gradually decreases until more inhibitor is added at 2500 seconds. As it can be seen the second addition of inhibitor leads to abrupt increase of potential and it sinks within 10 seconds to the level, which is lower than before the second addition. It is shown that stirring the system leads to higher potential and turning off the stirring leads to the plateau of the potential, which indicates a quasi equilibrium state. From this it can be concluded that stirring of approximately 400 seconds has dramatic influence to reaching the quasi equilibrium state. This effect can be lead back to the fact that the stirring promotes the inhibitor to be spread well in the system. Without the stirring the distribution of inhibitor molecules is dependent solely on the diffusion based on the concentration difference (Fick's law).



(a) Not stirred and inhibitor added twice. (b) Stirred and stopped stirring.

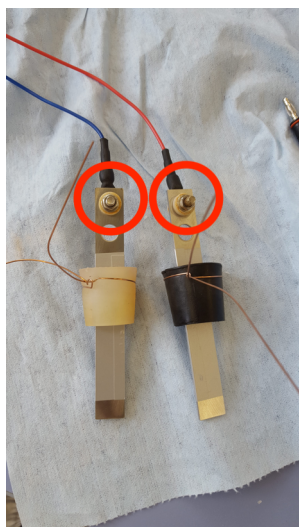
Figure 77: Record of open circuit potential in atmospheric condition (without CO₂).

Furthermore, the time point of inhibitor addition was tuned: it was introduced 20 minutes after the initiation of OCP measurement, instead of 5 minutes. By elongating this term, the coupons have more time to reach the quasi steady state without the inhibitor.

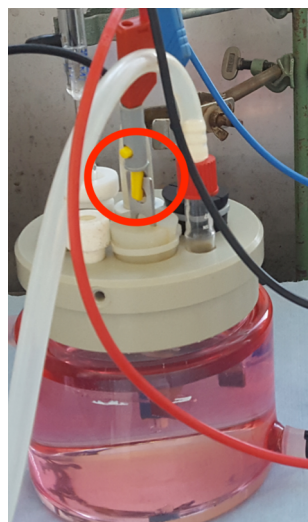
4.6.3 Cable setting

The length of the cable connecting the coupons to the potentiostat was shortened, by replacing the metal o-ring attached to another wire by crocodile clip. The importance of cables used for the measurements were expressed and studied by Ali(2013) [53]. His work has shown that phase angle measurement with a "bad" cable consists of spikes and when "better" cables were used much smoother curve was achieved [53]. Furthermore, it is known, that cable length and signal amplitude have effects on the region of accuracy of impedances and frequencies [54]. The study of Gamry instruments confirms the associa-

tion between the cable length and decrease of maximum applied frequency and maximum impedance limit. This phenomenon was explained by the increased resistance of the cable [54]. In order to avoid any possible cable effects the cable setting was changed (see the Figure 78).



(a)



(b)

Figure 78: Cables connecting the samples to the potentiostat, (a) before and (b) after the change.

5 Conclusions

The aim of the thesis was to study efficiency of corrosion inhibitors. The first step was to select inhibitors to do experiments with. The inhibitors were chosen based on the autoclave weight loss measurements and their toxicity. Then, C1020 steel with known surface area was immersed in 15% and 27% HCl at different temperature, and also inhibitor concentrations were varied. It was found that corrosion rate was decreased when higher dose of inhibitor concentration was added in all conditions and the corrosion rate increased with higher temperature and acid concentration. Inhibitor C, E and I had the highest inhibition efficiency, ranging from 95.59% to 99.98%. Inhibitor E showed the least change of IE regardless of the HCl concentration. Inhibitor D had higher IE than the reference substance butindiol at room temperature, however when the temperature was increased to 77°C its IE sank even below butindiol. As the inhibitor efficiency of each three inhibitors (Inhibitor C, E and I) is within the similar range, their corrosion rate was also compared. At room temperature in 15% HCl Inhibitor C and I showed the lowest corrosion rate when they were added 0.1% and 0.5% respectively. In acid concentration of 28 % at room temperature Inhibitor E (0.1%) and Inhibitor C (0.5% and 2%) had the lowest corrosion rate. Inhibitor C had the lowest corrosion rate at 77°C in 15 and 28%.

Polarization measurements were carried out in 15% HCl at room temperature (with and without carbon dioxide) and 50°C. In this measurement it was found that all corrosion inhibitors are mixed type, decreasing anodic and cathodic current density and with higher inhibitor concentration both current densities sank even more. At room temperature Inhibitor I had significant shift of E_{corr} to a more positive potential compare to other inhibitors and the shift was bigger when the concentration was increased. When CO_2 was added Inhibitor C and E had lower anodic and cathodic density current than without CO_2 . However, in case of Inhibitor I the cathodic curve was slightly higher when CO_2 was added and the anodic curve was not significantly effected by the presence of CO_2 .

Before executing electrochemical impedance spectroscopy (EIS), open circuit potential (OCP) was measured to determine for the quasi-steady state of the systems. Inhibitor efficiencies calculated from EIS data were all above 94% and it was considered as inadequate method to compare IE of inhibitors calculated from EIS measurements to claim which of these can inhibit corrosion the best. Thus, their normalized polarization resistance R_{pn} was compared instead. At room temperature and 50°C Inhibitor I (0.1%) proved to be the best inhibitor, with R_{pn} higher than the double of Inhibitor C and E.

When the inhibitor was added with 0.5% concentration at room temperature Inhibitor I had the highest R_{pn} as well. However, in carbon dioxide environment Inhibitor E showed the best corrosion inhibition, whereas Inhibitor I the worst.

Beside determining which inhibitor has better performance in inhibiting corrosion, developing a method to improve the repeatability of EIS measurements was one of the aims. The immersion depth of coupons in the electrolyte was adjusted so that a coupon was dipped in the electrolyte for only 1cm. Before starting a blank measurement, a pair of coupon was immersed in the electrolyte 5 minute long, however the duration was extended to 20 minutes. The duration of OCP measurement was extended from 45 minutes without stirring to 60 minutes with stirring. The cable setting was changed so that the coupons were connected to the potentiostat with only one cable and a crocodile clamp. Furthermore, it was studied how the way of adding inhibitor affects the repeatability of EIS measurements. Inhibitors were diluted either in 15% HCl or methanol or added directly with a pipette. However, no homogeneous solution could be reached when inhibitors were mixed with HCl or methanol, thus inhibitors were added directly. EIS measurements showed it depends on inhibitor and the experimental conditions how well EIS data can be reproduced. At room temperature EIS data of butindiol and all inhibitors except Inhibitor D could be reproduced well, however when the temperature was elevated to 50°C, EIS data of Inhibitor D and I could not be reproduced. When CO₂ was added in the electrolyte at room temperature, the repeatability of Inhibitor C was better compared to Inhibitor E and I due to the zigzag patterns. At room temperature when the inhibitor was added with 0.5% without CO₂ the zigzag pattern was so severe, that no significant reproducibility could be observed.

References

- [1] Brongers M. Thompson N. Virmani Y. Payer J. Koch, G. Corrosion cost and preventive strategies in the united states (nace international). 2002.
- [2] Liu Z Li Z Du C Dong C. Li X, Zhang D. Share corrosion data. *Nature*, 57(527):441, 2015.
- [3] B. Zhao. Qingdao pipeline explosion: introductions and reflections. *Natural Hazards*, 74(2):1299–1305, Nov 2014.
- [4] R. Dorothy G.Brindha M. Pandiarajan Abdulameed Al-Hashem S. Santhana Prabha, R. Joseph Rathish and S.Rajendran. Corrosion problems in petroleum industry and their solution. volume 3, pages 300–307. 2014.
- [5] V.S. Sastri. 5 - corrosion processes and the use of corrosion inhibitors in managing corrosion in underground pipelines. In Mark E. Orazem, editor, *Underground Pipeline Corrosion*, pages 127 – 165. Woodhead Publishing, 2014.
- [6] Steel Market Intelligence GmbH. The future of corrosion resistant steels and alloys in the oil and gas industry. *Stainless Steel World*, pages 1–3, 2013.
- [7] M. B. Kermani and A. Morshed. Carbon dioxide corrosion in oil and gas production—a compendium. *CORROSION*, 59(8):659–683, 2003.
- [8] A.M. Alsabagh, M.A. Migahed, and Hayam S. Awad. Reactivity of polyester aliphatic amine surfactants as corrosion inhibitors for carbon steel in formation water (deep well water). *Corrosion Science*, 48(4):813 – 828, 2006.
- [9] William Villamizar, M Casales, J Gonzalez-Rodriguez, and Lissette Martinez. Co2 corrosion inhibition by hydroxyethyl, aminoethyl, and amidoethyl imidazolines in water–oil mixtures. *Journal of Solid State Electrochemistry*, 11:619–629, 02 2007.
- [10] Corrosion in the oil industry. 6.
- [11] Mary Barrett. Documenting past oilfield arsenic corrosion documenting past oilfield arsenic corrosion inhibitor usage: a pit groundwater example inhibitor usage: a pit groundwater example from lake st. john field, la from lake st. john field, la, 05 2018.
- [12] Matjaž Finšgar and Jennifer Jackson. Application of corrosion inhibitors for steels in acidic media for the oil and gas industry: A review. *Corrosion Science*, 86:17 – 41, 2014.

- [13] Sunder Ramachandran. 19 - corrosion inhibitors—advancements in testing. In A.M. El-Sherik, editor, *Trends in Oil and Gas Corrosion Research and Technologies*, Woodhead Publishing Series in Energy, pages 455 – 469. Woodhead Publishing, Boston, 2017.
- [14] R. Winston Revie and Herbert Henry Uhlig. *Corrosion and corrosion control: an introduction to corrosion science and engineering*. Wiley-Interscience, 2008.
- [15] Peter Zarras and John D. Stenger-Smith. Chapter 3 - smart inorganic and organic pretreatment coatings for the inhibition of corrosion on metals/alloys. In Atul Tiwari, James Rawlins, and Lloyd H. Hihara, editors, *Intelligent Coatings for Corrosion Control*, pages 59 – 91. Butterworth-Heinemann, Boston, 2015.
- [16] K. Sridharan and T.R. Allen. 12 - corrosion in molten salts. In Frédéric Lantelme and Henri Groult, editors, *Molten Salts Chemistry*, pages 241 – 267. Elsevier, Oxford, 2013.
- [17] J. Zhang, P. Hosemann, and S. Maloy. Models of liquid metal corrosion. *Journal of Nuclear Materials*, 404(1):82 – 96, 2010.
- [18] P.R. Roberge. *Corrosion Engineering: Principles and Practice*. McGraw-Hill Education, 2008.
- [19] Lekan Taofeek Popoola, Alhaji Shehu Grema, Ganiyu Kayode Latinwo, Babagana Gutti, and Adebori Saheed Balogun. Corrosion problems during oil and gas production and its mitigation. *International Journal of Industrial Chemistry*, 4(1):35, Sep 2013.
- [20] J. Kruger. Corrosion of metals: Overview. In K.H. Jürgen Buschow, Robert W. Cahn, Merton C. Flemings, Bernhard Ilshner, Edward J. Kramer, Subhash Mahajan, and Patrick Veyssi re, editors, *Encyclopedia of Materials: Science and Technology*, pages 1701 – 1706. Elsevier, Oxford, 2001.
- [21] Ramazan Asmatulu Navid Rashidi, Seyed Alavi-Soltani*. Crevice corrosion theory, mechanisms and prevention methods. *Proceedings of the 3rd Annual GRASP Symposium, Wichita State University*, pages 215–216, 2007.
- [22] Graham E.C. Bell Mersedeh Akhoondan. Fastener corrosion. *Structure magazine*, pages 74–75, 2016.

- [23] K Nalli. Corrosion and its mitigation in the oil and gas industry-an overview. *Petro-Min Pipeliner*, pages 10–16, 01 2010.
- [24] A.R. Hendrickson and E.N. Alderman. Acidizing: Fact and fiction. *Paper PETSOC-7106, 22nd Annual Technical Meeting of the Petroleum Society of CIM in Banff*, 6:2–5, 06 1971.
- [25] Seyed Bassir and Khalil Shahbazi. A comprehensive review of optimization of acidizing in sandstone/carbonate reservoirs. pages 1–10, 12 2016.
- [26] *Types of Corrosion Inhibitors*, chapter 10, pages 25–26. John Wiley and Sons, Ltd, 2017.
- [27] Camila G. Dariva and Alexandre F. Galio. Corrosion inhibitors – principles, mechanisms and applications. In M. Aliofkhazraei, editor, *Developments in Corrosion Protection*, chapter 16. IntechOpen, Rijeka, 2014.
- [28] Pierre R. Roberge. *Handbook of corrosion engineering*. McGraw-Hill, 2000.
- [29] S. Papavinasam. *Corrosion Inhibitors*, chapter 71, pages 1021–1032. John Wiley and Sons, Ltd, 2011.
- [30] Alireza Bahadori. *Corrosion and materials selection: a guide for the chemical and petroleum industries*. John Wiley and Sons, Ltd., 2014.
- [31] Yu V. Banakhevych, Oksana Hembara, and O E. Andreikiv. Numerical analysis of the kinetics of propagation of hydrogen blisters in the oil-and-gas equipment. *Materials Science*, 45:626–637, 09 2009.
- [32] Shaowei Chen. 2 - practical electrochemical cells. In Cynthia G. Zoski, editor, *Handbook of Electrochemistry*, pages 33 – 56. Elsevier, Amsterdam, 2007.
- [33] Noémie Elgrishi, Kelley J. Rountree, Brian D. McCarthy, Eric S. Rountree, Thomas T. Eisenhart, and Jillian L. Dempsey. A practical beginner’s guide to cyclic voltammetry. *Journal of Chemical Education*, 95(2):197–206, 2018.
- [34] Florian Mansfeld. Use of electrochemical impedance spectroscopy for the study of corrosion protection by polymer coatings. *Journal of Applied Electrochemistry*, 25:187–202, 01 1995.

- [35] Arlavinda Rezqita, Raad Hamid, S Schwarz, Hermann Kronberger, and A Trifonova. Conductive additive for si/mesoporous carbon anode for li-ion batteries: Commercial graphite vs carbon black c65. *ECS Transactions*, 66:17–27, 08 2015.
- [36] Carmelo Brunetto, Antonino Moschetto, and Giuseppe Tina. Pem fuel cell testing by electrochemical impedance spectroscopy. *Electric Power Systems Research*, 79(1):17 – 26, 2009.
- [37] David TURCIO-ORTEGA, Pandiyan Thangarasu, and E García-Ochoa. Electrochemical impedance spectroscopy (eis) study of the film formation of 2-imidazoline derivatives on carbon steel in acid solution. *Materials Science*, 13, 06 2007.
- [38] Peterspm P Loveday, D and B Rodgers. Evaluation of organic coatings with electrochemical impedance spectroscopy - part 1: Fundamentals of electrochemical impedance spectroscopy. *JCT CoatingsTech*, pages 46–52, 8 2004.
- [39] Madalina Ciobanu, Jeremy P. Wilburn, Morgan L. Krim, and David E. Cliffl. 1 - fundamentals. In Cynthia G. Zoski, editor, *Handbook of Electrochemistry*, pages 3 – 29. Elsevier, Amsterdam, 2007.
- [40] A.E. Hughes, J M C Mol, M.L. Zheludkevich, and Rudolph G. Buchheit. *Active Protective Coatings: New-Generation Coatings for Metals*. 01 2016.
- [41] E. McCafferty and James V. McArdle. Corrosion inhibition of iron in acid solutions by biological siderophores. *Journal of The Electrochemical Society*, 142(5):1447–1453, 1995.
- [42] Revathi Mohan and Abraham Joseph. Corrosion protection of mild steel in hydrochloric acid up to 313k using propyl benzimidazole: Electroanalytical, adsorption and quantum chemical studies. *Egyptian Journal of Petroleum*, 27(1):11 – 20, 2018.
- [43] Amit Bansal, Apurbba Kumar Sharma, and Pradeep Kumar. Galvanic corrosion behavior of microwave welded and post-weld heat-treated inconel-718 joints. *Journal of Materials Engineering and Performance*, 26(5):2322–2330, May 2017.
- [44] L. M. Fernandez Diaz, O. Bendick, C. Ostwald, and T. Appel. Study of the influence of some organics as thiourea derivatives and butindiol in steel pickling baths. *Materials and Corrosion*, 57(9):689–695, 2006.

- [45] Z D. Cui, Shuilin Wu, S L. Zhu, and X J. Yang. Study on corrosion properties of pipelines in simulated produced water saturated with supercritical co₂. *Applied Surface Science - APPL SURF SCI*, 252:2368–2374, 01 2006.
- [46] Yarong Song, Guangming Jiang, Ying Chen, Peng Zhao, and Yimei Tian. Effects of chloride ions on corrosion of ductile iron and carbon steel in soil environments. In *Scientific Reports*, 2017.
- [47] Anees Khadom, Aprael Yaro, Abdul Amir, H Kadum, and Ahmed S. AlTaie. The effect of temperature and acid concentration on corrosion of low carbon steel in hydrochloric acid media. *American Journal of Applied Sciences*, 6:1403–1409, 07 2009.
- [48] Xujin Sun and Liangmin Yu. Investigation of polyacrylamide containing capsaicin monomer as a novel corrosion inhibitor for mild steel in hydrochloric acid. *Materials and Corrosion*, 69(8):1095–1103, mar 2018.
- [49] Fathul Sahrani, Madzlan Aziz, Zaharah Ibrahim, and Adibah Yahya. Potentiodynamic polarization study of type 316l and 316lvm stainless steels for surgical implants in simulated body fluids. *Journal of Chemical and Pharmaceutical Research*, 4:203–208, 2008.
- [50] Ahmed A. Al-Amiery, Abdul Amir H. Kadhum, Abdul Hameed M. Alobaidy, Abu Bakar Mohamad, and Pua Soh Hoon. Novel corrosion inhibitor for mild steel in hcl. *Materials*, 7(2):662–672, 2014.
- [51] C. K. Behera Mohd Talha and O. P. Sinha. Open circuit potential study of stainless steel in environment containing marine sulphate-reducing bacteria. *Sains Malaysiana*, 37, 12 2012.
- [52] Roland Tolulope Loto. Electrochemical analysis of the corrosion inhibition effect of trypsin complex on the pitting corrosion of 420 martensitic stainless steel in 2m h₂so₄ solution. *PLOS ONE*, 13(4):1–13, 04 2018.
- [53] Mohammad Ali. Studies of the use of electrochemical impedance spectroscopy to characterize and assess the performance of lacquers used to protect aluminum sheet and can ends, 2013.
- [54] Inc. Gamry Instruments. *How Cabling and Signal Amplitudes Affect EIS Results*, Rev. 1.0 11/9/2016 (accessed January 30, 2019).

List of Figures

1	Schematic description of crevice corrosion [18].	6
2	Galvanic corrosion [22].	6
3	10
4	An illustration of a three electrode set-up [33].	11
5	Delayed response [38].	12
6	Typical Bode diagram. Frequency was varied from 0.01 Hz to 80160 Hz. .	14
7	Nyquist plot. Frequency was varied from 0.01 Hz to 80160 Hz.	15
8	Open circuit potential as a function of time of an inhibitor in 15% HCl at room temperature.	16
9	Polarization curves for iron in 1 M HCl in absence of oxygen [41].	17
10	Potentiodynamic polarization curves of metals with different heat treatment [43].	18
11	Flasks with lids in the water bath.	20
12	A flask containing two coupons submerged in 15 wt.% HCl solution and 0.1 vol.% butindiol and the sealed opening with two holes.	20
13	Components of an autoclave and the metal coupons on the sample holder. .	21
14	Autoclaves placed on the wheel apparatus.	22
15	Polished sample.	22
16	A coupon covered with a film.	23
17	A coupon tip wrapped with PTFE tape and consequently applied resin. .	23
18	A prepared coupon, which can be used for EIS measurements.	24
19	Electrodes mounted in conical frustum shaped rubber.	25
20	Platinum wire counter electrode for polarization curve measurements. . .	25
21	Experimental setup for polarization measurement : a) Ag/AgCl reference electrode, b1) counter electrode, b2) working electrode for EIS and OCP measurements, c) platinum wire counter electrode, d) glass double-wall jacketed cell, e) magnetic stirrer.	26
22	Cleaning gas washing bottle head with acetone using a pump.	26
23	Cut sample and the sample holder.	28
24	Mounted sample before and after the polishing.	28
25	Autoclave experiments in two different medium: (a) osmosis water with 20 bar CO ₂ (no Cl ⁻ present), (b) pH3-Buffer with 5 bar N ₂ (Cl ⁻ present).	30
26	32

27	Inhibitor efficiency in 15% HCl in room temperature. The tested concentrations of inhibitors were 0.1 vol.% and 0.5 vol.%.	33
28	Inhibitor efficiency in 28% HCl in room temperature. The tested concentrations of inhibitors were 0.1 vol.%, 0.5 vol.% and 2 vol.%.	33
29	Inhibitor efficiency in 15% HCl at 77°C. The tested concentrations of inhibitors were 0.1 vol.% and 0.5 vol.%.	34
30	Inhibitor efficiency in 28% HCl at 77°C. The tested concentrations of inhibitors were 0.5 vol.% and 2 vol.%.	34
31	Tafel polarization curves of different inhibitors with 0.1 vol.% measured at room temperature in the open air without CO ₂	37
32	Tafel polarization curves of different inhibitors with 0.5 vol.% measured at room temperature in the open air without CO ₂	38
33	Comparison of polarization curves of each inhibitors with different concentrations in 15 % HCl at room temperature without CO ₂	38
34	Comparison of polarization curves of each inhibitors (0.1 vol.%) with and without CO ₂ in 15% HCl at room temperature.	39
35	Tafel polarization curves of different inhibitors with 0.1 vol.% measured at room temperature, while carbon dioxide gas was purged into the electrolyte.	40
36	Tafel polarization curves of different inhibitors with 0.1 vol.% measured at 50°C without CO ₂	40
37	OCP curve in 0.1% Inhibitor E at 50°C.	41
38	(a) Nyquist plot and (b) Bode plot of Inhibitor E at 50°C with 0.1% concentration.	42
39	OCP curve in 0.1% Inhibitor I at RT.	42
40	Nyquist plot and Bode plot of Inhibitor I at room temperature with 0.1% concentration.	43
41	OCP curve in 0.1% Inhibitor E at RT in CO ₂ saturated hydrochloric acid solution.	43
42	OCP curve in 0.1% Inhibitor E at RT without CO ₂	43
43	OCP curve in 0.5% Inhibitor E at RT without CO ₂	44
44	Equivalent electric circuit model used to fit impedance data.	45
45	Fitted impedance data of (a) Inhibitor D at room temperature (b) Inhibitor I at room temperature with 0.5% concentration without CO ₂	45
46	Nyquist plot for C1020 steel in 15% HCl solutions without CO ₂ at room temperature (a) and 50°C (b).	46

47	Nyquist plot for C1020 steel in 15% HCl solutions with 0.1% inhibitor at different experimental conditions.	47
48	OCP measurement of Inhibitor I at 50°C with 0.1% inhibitor.	48
49	OCP measurement of Inhibitor B at 50°C with 0.1% inhibitor.	48
50	Nyquist plot of Inhibitor B at 50°C with 0.1% inhibitor.	48
51	Nyquist plot of a dummy cell measured with two different instruments.	49
52	Nyquist plot for C1020 steel in 15% HCl solutions in different experimental conditions.	51
53	Inhibitor B at room temperature without CO ₂ with 0.1% concentration.	53
54	Inhibitor C at room temperature and 50°C without CO ₂ with 0.1% concentration.	53
55	Inhibitor D at room temperature without CO ₂ with 0.1% concentration.	53
56	Inhibitor E at room temperature without CO ₂ with 0.1% concentration.	54
57	Inhibitor I at room temperature without CO ₂ with 0.1% concentration.	54
58	Butindiol at room temperature without CO ₂ with 0.1% concentration.	54
59	Butindiol at 50°C without CO ₂ with 0.1% concentration.	55
60	Inhibitor B at 50°C without CO ₂ with 0.1% concentration.	55
61	Inhibitor C at 50°C without CO ₂ with 0.1% concentration.	56
62	Inhibitor D at 50°C without CO ₂ with 0.1% concentration.	56
63	Inhibitor E at 50°C without CO ₂ with 0.1% concentration.	57
64	Inhibitor I at 50°C without CO ₂ with 0.1% concentration.	57
65	Inhibitor E at room temperature with CO ₂ with 0.1% concentration.	58
66	Inhibitor I at room temperature with CO ₂ with 0.1% concentration.	58
67	Two independent measurements of Inhibitor C at room temperature with CO ₂ with 0.1% concentration.	59
68	Two independent measurements of Inhibitor I at room temperature without CO ₂ with 0.5% concentration.	59
69	Inhibitor E at room temperature without CO ₂ with 0.5 % concentration.	60
70	Metal coupon and acrylic resin embedded in the black resin.	61
71	Metal coupon under the microscope after finishing experiments. The coupon is shown as white, lighter grey part is the resin for embedding and the darker grey area is the acrylic resin.	62
72	Part of the metal coupon, which was dipped in the hydrochloric acid. The left picture was better lit than the right one.	62
73	Part of a metal coupon, which did not have any contact with the hydrochloric acid. The left picture was better lit than the right one.	62

74	Inhibitor E mixed into hydrochloric acid.	63
75	Inhibitor D mixed into hydrochloric acid.	64
76	Inhibitor D mixed into methanol.	64
77	Record of open circuit potential in atmospheric condition (without CO ₂).	65
78	Cables connecting the samples to the potentiostat, (a) before and (b) after the change.	66
79	OCP curve in 0.1% Inhibitor B at RT.	81
80	OCP curve in 0.1% Inhibitor B at 50°C.	81
81	OCP curve in 0.1% Inhibitor C at RT.	81
82	OCP curve in 0.5% Inhibitor C at RT.	81
83	OCP curve in 0.1% Inhibitor C at RT in saturated CO ₂ hydrochloric acid solution.	82
84	OCP curve in 0.1% Inhibitor C at 50°C.	82
85	OCP curve in 0.1% Inhibitor D at RT.	82
86	OCP curve in 0.1% Inhibitor D at 50°C.	82
87	OCP curve in 0.5% Inhibitor I at RT.	83
88	OCP curve in 0.1% Inhibitor I at RT in saturated CO ₂ hydrochloric acid solution.	83
89	OCP curve in 0.1% Inhibitor I at 50°C.	83
90	OCP curve in 0.1% butindiol at RT.	83
91	OCP curve in 0.1% butindiol at 50°C.	84

List of Tables

1	Overview of executed blank measurements with varying temperature, concentration of medium and duration.	19
2	Overview of executed weight loss measurements with inhibitors.	21
3	Corrosion rate v and inhibitor efficiency of C1020 alloy in 15% HCl at room temperature. The tested concentrations of inhibitors were 0.1 vol.% and 0.5 vol.%.	35
4	Corrosion rate v and inhibitor efficiency of C1020 alloy in 28% HCl at room temperature. The tested concentrations of inhibitors were 0.1 vol.%, 0.5 vol.% and 2 vol.%.	36
5	Corrosion rate v and inhibitor efficiency of C1020 alloy in 15% HCl at 77°C. The tested concentrations of inhibitors were 0.1 vol.% and 0.5 vol.%. . .	36
6	Corrosion rate v and inhibitor efficiency of C1020 alloy in 28% HCl at 77°C. The tested concentrations of inhibitors were 0.5 vol.% and 2 vol.%. . . .	36
7	Inhibitor efficiency of inhibitors (0.1 vol.%) measured with EIS at room temperature and 50°C.	49
8	Normalized polarization resistance of inhibitors (0.1 vol.%) measured with EIS at room temperature and 50°C.	50
9	Protection rate of inhibitors (0.5 vol.%) measured with EIS at room temperature.	51
10	Normalized polarization resistance of inhibitors (0.5 vol.%) measured with EIS at room temperature.	52
11	Protection rate of inhibitors (0.1 vol.%) measured with EIS at room temperature with CO ₂ bubbling.	52
12	Normalized polarization resistance of inhibitors (0.1 vol.%) measured with EIS at room temperature with CO ₂ bubbling.	52

List of Abbreviations

AC Alternating current

CPE Constant phase element

EIS Electrochemical impedance spectroscopy

IE Inhibitor efficiency

OCP Open circuit potential

RT Room temperature

Appendix

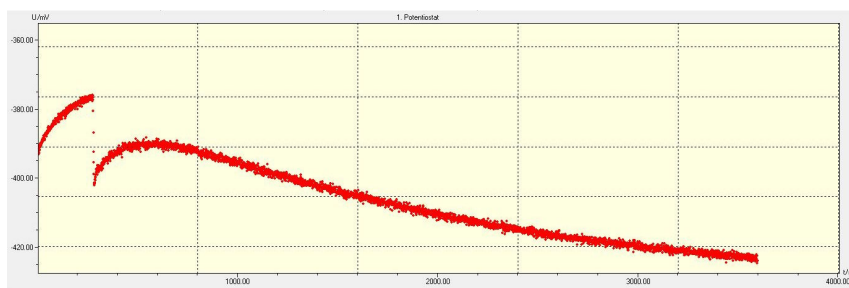


Figure 79: OCP curve in 0.1% Inhibitor B at RT.

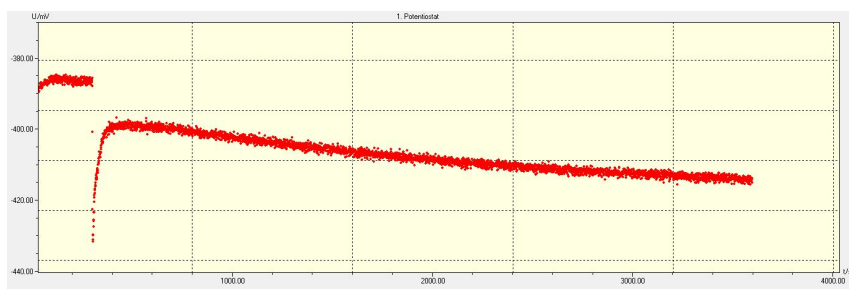


Figure 80: OCP curve in 0.1% Inhibitor B at 50°C.

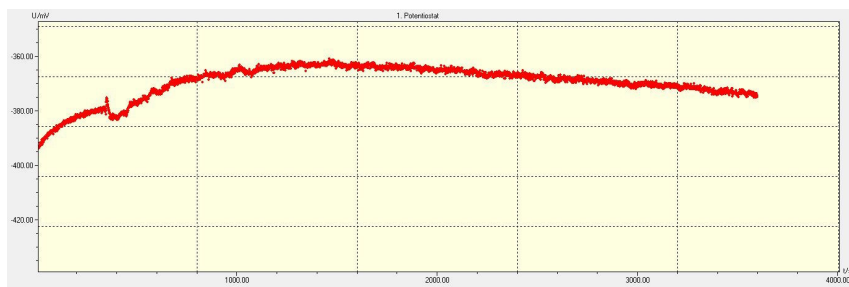


Figure 81: OCP curve in 0.1% Inhibitor C at RT.

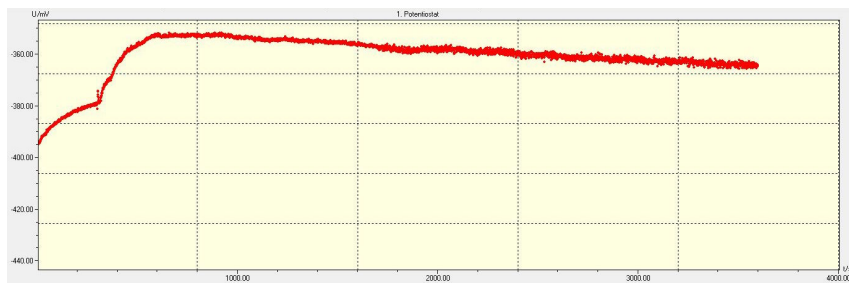


Figure 82: OCP curve in 0.5% Inhibitor C at RT.

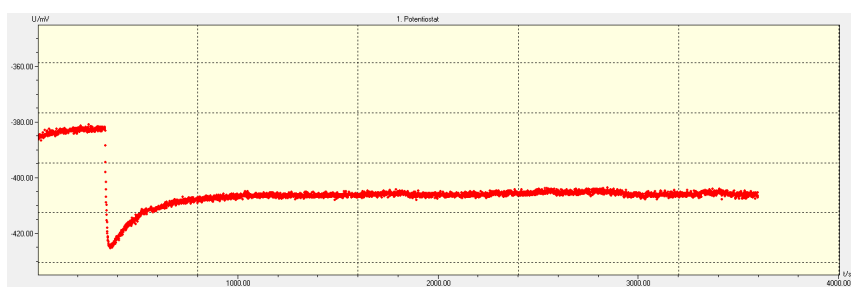


Figure 83: OCP curve in 0.1% Inhibitor C at RT in saturated CO₂ hydrochloric acid solution.

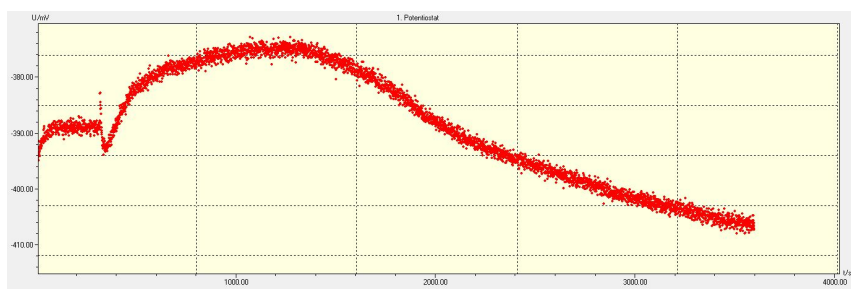


Figure 84: OCP curve in 0.1% Inhibitor C at 50°C.

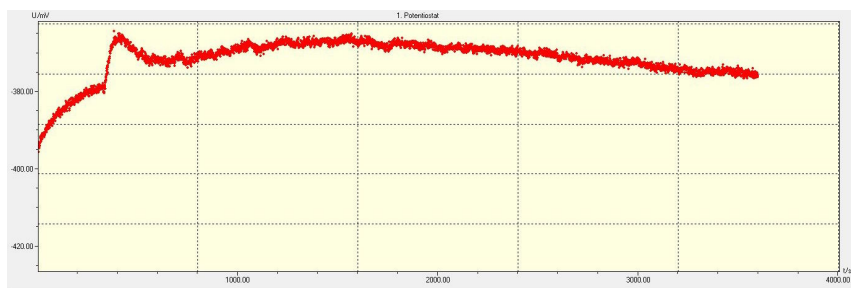


Figure 85: OCP curve in 0.1% Inhibitor D at RT.

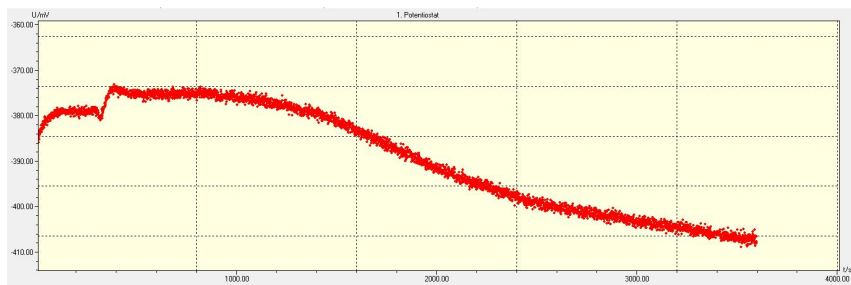


Figure 86: OCP curve in 0.1% Inhibitor D at 50°C.

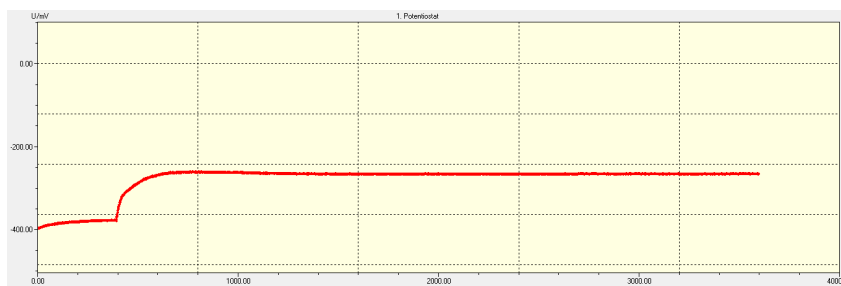


Figure 87: OCP curve in 0.5% Inhibitor I at RT.

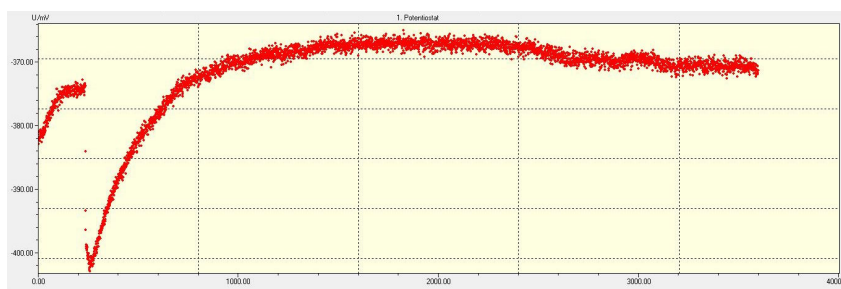


Figure 88: OCP curve in 0.1% Inhibitor I at RT in saturated CO₂ hydrochloric acid solution.



Figure 89: OCP curve in 0.1% Inhibitor I at 50°C.

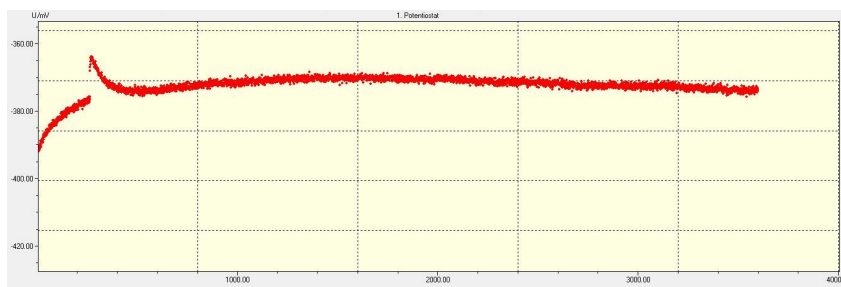


Figure 90: OCP curve in 0.1% butindiol at RT.

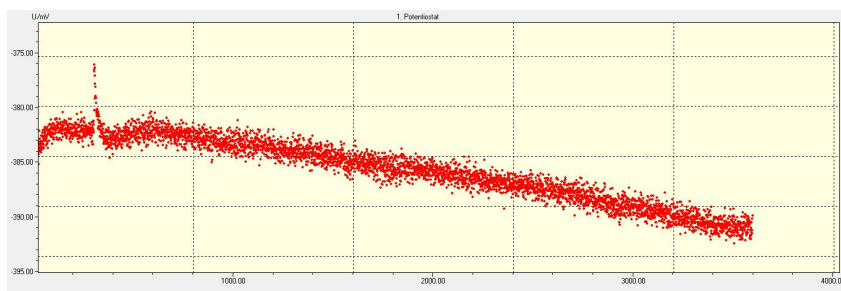


Figure 91: OCP curve in 0.1% butindiol at 50°C.